EUROPEAN ORGANIZATION FOR NUCLEAR RESEARCH

CERN–EP/2003-061

12 June 2003

Searches for Neutral Higgs Bosons in Extended Models

DELPHI Collaboration

Abstract

Searches for neutral Higgs bosons produced at LEP in association with Z bosons, in pairs and in the Yukawa process are presented in this paper. Higgs boson decays into b quarks, τ leptons, or other Higgs bosons are considered, giving rise to four-b, four-b+jets, six-b and four-τ final states, as well as mixed modes with b quarks and τ leptons. The whole mass domain kinematically accessible at LEP in these topologies is searched. The analysed data set covers both the LEP1 and LEP2 energy ranges and exploits most of the luminosity recorded by the DELPHI experiment. No convincing evidence for a signal is found, and results are presented in the form of mass-dependent upper bounds on coupling factors (in units of model-independent reference cross-sections) for all processes, allowing interpretation of the data in a large class of models.

(Accepted by Eur. Phys. J. C)

J.Abdallah[25], P.Abreu[22], W.Adam[51], P.Adzic[11], T.Albrecht[17], T.Alderweireld[2], R.Alemany-Fernandez[8], T.Allmendinger[17], P.P.Allport[23], U.Amaldi[29], N.Amapane[45], S.Amato[48], E.Anashkin[36], A.Andreazza[28], S.Andringa[22], N.Anjos[22], P.Antilogus[25], W-D.Apel[17], Y.Arnoud[14], S.Ask[26], B.Asman[44], J.E.Augustin[25], A.Augustinus[8], P.Baillon[8], A.Ballestrero[46], P.Bambade[20], R.Barbier[27], D.Bardin[16], G.J.Barker[17], A.Baroncelli[39], M.Battaglia[8], M.Baubillier[25], K-H.Becks[53], M.Begalli[6], A.Behrmann[53], E.Ben-Haim[20], N.Benekos[32], A.Benvenuti[5], C.Berat[14], M.Berggren[25], L.Berntzon[44], D.Bertrand[2], M.Besancon[40], N.Besson[40], D.Bloch[9], M.Blom[31], M.Bluj[52], M.Bonesini[29], M.Boonekamp[40], P.S.L.Booth[23], G.Borisov[21], O.Botner[49], B.Bouquet[20], T.J.V.Bowcock[23], I.Boyko[16], M.Bracko[43], R.Brenner[49], E.Brodet[35], P.Bruckman[18], J.M.Brunet[7], L.Bugge[33], P.Buschmann[53], M.Calvi[29], T.Camporesi[8], V.Canale[38], F.Carena[8], N.Castro[22], F.Cavallo[5], M.Chapkin[42], Ph.Charpentier[8], P.Checchia[36], R.Chierici[8], P.Chliapnikov[42], J.Chudoba[8], S.U.Chung[8], K.Cieslik[18], P.Collins[8], R.Contri[13], G.Cosme[20], F.Cossutti[47], M.J.Costa[50], D.Crennell[37], J.Cuevas[34], J.D'Hondt[2], J.Dalmau[44], T.da Silva[48], W.Da Silva[25], G.Della Ricca[47], A.De Angelis[47], W.De Boer[17], C.De Clercq[2], B.De Lotto[47], N.De Maria[45], A.De Min[36], L.de Paula[48], L.Di Ciaccio[38], A.Di Simone[39], K.Doroba[52], J.Drees[53,8], M.Dris[32], G.Eigen[4], T.Ekelof[49], M.Ellert[49], M.Elsing[8], M.C.Espirito Santo[22], G.Fanourakis[11], D.Fassouliotis[11,3], M.Feindt[17], J.Fernandez[41], A.Ferrer[50], F.Ferro[13], U.Flagmeyer[53], H.Foeth[8], E.Fokitis[32], F.Fulda-Quenzer[20], J.Fuster[50], M.Gandelman[48], C.Garcia[50], Ph.Gavillet[8], E.Gazis[32], R.Gokieli[8,52], B.Golob[43], G.Gomez-Ceballos[41], P.Goncalves[22], E.Graziani[39], G.Grosdidier[20], K.Grzelak[52], J.Guy[37], C.Haag[17], A.Hallgren[49], K.Hamacher[53], K.Hamilton[35], S.Haug[33], F.Hauler[17], V.Hedberg[26], M.Hennecke[17], H.Herr[8], J.Hoffman[52], S-O.Holmgren[44], P.J.Holt[8], M.A.Houlden[23], K.Hultqvist[44], J.N.Jackson[23], G.Jarlskog[26], P.Jarry[40], D.Jeans[35], E.K.Johansson[44], P.D.Johansson[44], P.Jonsson[27], C.Joram[8], L.Jungermann[17], F.Kapusta[25], S.Katsanevas[27], E.Katsoufis[32], G.Kernel[43], B.P.Kersevan[8,43], U.Kerzel[17], A.Kiiskinen[15], B.T.King[23], N.J.Kjaer[8], P.Kluit[31], P.Kokkinias[11], C.Kourkoumelis[3], O.Kouznetsov[16], Z.Krumstein[16], M.Kucharczyk[18], J.Lamsa[1], G.Leder[51], F.Ledroit[14], L.Leinonen[44], R.Leitner[30], J.Lemonne[2], V.Lepeltier[20], T.Lesiak[18], W.Liebig[53], D.Liko[51], A.Lipniacka[44], J.H.Lopes[48], J.M.Lopez[34], D.Loukas[11], P.Lutz[40], L.Lyons[35], J.MacNaughton[51], A.Malek[53], S.Maltezos[32], F.Mandl[51], J.Marco[41], R.Marco[41], B.Marechal[48], M.Margoni[36], J-C.Marin[8], C.Mariotti[8], A.Markou[11], C.Martinez-Rivero[41], J.Masik[12], N.Mastroyiannopoulos[11], F.Matorras[41], C.Matteuzzi[29], F.Mazzucato[36], M.Mazzucato[36], R.Mc Nulty[23], C.Meroni[28], E.Migliore[45], W.Mitaroff[51], U.Mjoernmark[26], T.Moa[44], M.Moch[17], K.Moenig[8,10], R.Monge[13], J.Montenegro[31], D.Moraes[48], S.Moreno[22], P.Morettini[13], U.Mueller[53], K.Muenich[53], M.Mulders[31], L.Mundim[6], W.Murray[37], B.Muryn[19], G.Myatt[35], T.Myklebust[33], M.Nassiakou[11], F.Navarria[5], K.Nawrocki[52], R.Nicolaidou[40], M.Nikolenko[16,9], A.Oblakowska-Mucha[19], V.Obraztsov[42], A.Olshevski[16], A.Onofre[22], R.Orava[15], K.Osterberg[15], A.Ouraou[40], A.Oyanguren[50], M.Paganoni[29], S.Paiano[5], J.P.Palacios[23], H.Palka[18], Th.D.Papadopoulou[32], L.Pape[8], C.Parkes[24], F.Parodi[13], U.Parzefall[8], A.Passeri[39], O.Passon[53], L.Peralta[22], V.Perepelitsa[50], A.Perrotta[5], A.Petrolini[13], J.Piedra[41], L.Pieri[39], F.Pierre[40], M.Pimenta[22], E.Piotto[8], T.Podobnik[43], V.Poireau[8], M.E.Pol[6], G.Polok[18], V.Pozdniakov[16], N.Pukhaeva[2,16], A.Pullia[29], J.Rames[12], A.Read[33], P.Rebecchi[8], J.Rehn[17], D.Reid[31], R.Reinhardt[53], P.Renton[35], F.Richard[20], J.Ridky[12], M.Rivero[41], D.Rodriguez[41], A.Romero[45], P.Ronchese[36], P.Roudeau[20], T.Rovelli[5], V.Ruhlmann-Kleider[40], D.Ryabtchikov[42], A.Sadovsky[16], L.Salmi[15], J.Salt[50], C.Sander[17], A.Savoy-Navarro[25], U.Schwickerath[8], A.Segar[35], R.Sekulin[37], M.Siebel[53], A.Sisakian[16], G.Smadja[27], O.Smirnova[26], A.Sokolov[42], A.Sopczak[21], R.Sosnowski[52], T.Spassov[8], M.Stanitzki[17], A.Stocchi[20], J.Strauss[51], B.Stugu[4], M.Szczekowski[52], M.Szeptycka[52], T.Szumlak[19], T.Tabarelli[29], A.C.Taffard[23], F.Tegenfeldt[49], J.Timmermans[31], L.Tkatchev[16], M.Tobin[23], S.Todorovova[12], B.Tome[22], A.Tonazzo[29], P.Tortosa[50], P.Travnicek[12], D.Treille[8], G.Tristram[7], M.Trochimczuk[52], C.Troncon[28], M-L.Turluer[40], I.A.Tyapkin[16], P.Tyapkin[16], S.Tzamarias[11], V.Uvarov[42], G.Valenti[5], P.Van Dam[31], J.Van Eldik[8], A.Van Lysebetten[2], N.van Remortel[2], I.Van Vulpen[8], G.Vegni[28], F.Veloso[22], W.Venus[37], P.Verdier[27], V.Verzi[38], D.Vilanova[40], L.Vitale[47], V.Vrba[12], H.Wahlen[53], A.J.Washbrook[23], C.Weiser[17], D.Wicke[8],

J.Wickens[2], G.Wilkinson[35], M.Winter[9], M.Witek[18], O.Yushchenko[42], A.Zalewska[18], P.Zalewski[52], D.Zavrtanik[43], V.Zhuravlov[16], N.I.Zimin[16], A.Zintchenko[16], M.Zupan[11]

[1]Department of Physics and Astronomy, Iowa State University, Ames IA 50011-3160, USA
[2]Physics Department, Universiteit Antwerpen, Universiteitsplein 1, B-2610 Antwerpen, Belgium
and IIHE, ULB-VUB, Pleinlaan 2, B-1050 Brussels, Belgium
and Faculté des Sciences, Univ. de l'Etat Mons, Av. Maistriau 19, B-7000 Mons, Belgium
[3]Physics Laboratory, University of Athens, Solonos Str. 104, GR-10680 Athens, Greece
[4]Department of Physics, University of Bergen, Allégaten 55, NO-5007 Bergen, Norway
[5]Dipartimento di Fisica, Università di Bologna and INFN, Via Irnerio 46, IT-40126 Bologna, Italy
[6]Centro Brasileiro de Pesquisas Físicas, rua Xavier Sigaud 150, BR-22290 Rio de Janeiro, Brazil
and Depto. de Física, Pont. Univ. Católica, C.P. 38071 BR-22453 Rio de Janeiro, Brazil
and Inst. de Física, Univ. Estadual do Rio de Janeiro, rua São Francisco Xavier 524, Rio de Janeiro, Brazil
[7]Collège de France, Lab. de Physique Corpusculaire, IN2P3-CNRS, FR-75231 Paris Cedex 05, France
[8]CERN, CH-1211 Geneva 23, Switzerland
[9]Institut de Recherches Subatomiques, IN2P3 - CNRS/ULP - BP20, FR-67037 Strasbourg Cedex, France
[10]Now at DESY-Zeuthen, Platanenallee 6, D-15735 Zeuthen, Germany
[11]Institute of Nuclear Physics, N.C.S.R. Demokritos, P.O. Box 60228, GR-15310 Athens, Greece
[12]FZU, Inst. of Phys. of the C.A.S. High Energy Physics Division, Na Slovance 2, CZ-180 40, Praha 8, Czech Republic
[13]Dipartimento di Fisica, Università di Genova and INFN, Via Dodecaneso 33, IT-16146 Genova, Italy
[14]Institut des Sciences Nucléaires, IN2P3-CNRS, Université de Grenoble 1, FR-38026 Grenoble Cedex, France
[15]Helsinki Institute of Physics, P.O. Box 64, FIN-00014 University of Helsinki, Finland
[16]Joint Institute for Nuclear Research, Dubna, Head Post Office, P.O. Box 79, RU-101 000 Moscow, Russian Federation
[17]Institut für Experimentelle Kernphysik, Universität Karlsruhe, Postfach 6980, DE-76128 Karlsruhe, Germany
[18]Institute of Nuclear Physics PAN,Ul. Radzikowskiego 152, PL-31142 Krakow, Poland
[19]Faculty of Physics and Nuclear Techniques, University of Mining and Metallurgy, PL-30055 Krakow, Poland
[20]Université de Paris-Sud, Lab. de l'Accélérateur Linéaire, IN2P3-CNRS, Bât. 200, FR-91405 Orsay Cedex, France
[21]School of Physics and Chemistry, University of Lancaster, Lancaster LA1 4YB, UK
[22]LIP, IST, FCUL - Av. Elias Garcia, 14-1^{o}, PT-1000 Lisboa Codex, Portugal
[23]Department of Physics, University of Liverpool, P.O. Box 147, Liverpool L69 3BX, UK
[24]Dept. of Physics and Astronomy, Kelvin Building, University of Glasgow, Glasgow G12 8QQ
[25]LPNHE, IN2P3-CNRS, Univ. Paris VI et VII, Tour 33 (RdC), 4 place Jussieu, FR-75252 Paris Cedex 05, France
[26]Department of Physics, University of Lund, Sölvegatan 14, SE-223 63 Lund, Sweden
[27]Université Claude Bernard de Lyon, IPNL, IN2P3-CNRS, FR-69622 Villeurbanne Cedex, France
[28]Dipartimento di Fisica, Università di Milano and INFN-MILANO, Via Celoria 16, IT-20133 Milan, Italy
[29]Dipartimento di Fisica, Univ. di Milano-Bicocca and INFN-MILANO, Piazza della Scienza 2, IT-20126 Milan, Italy
[30]IPNP of MFF, Charles Univ., Areal MFF, V Holesovickach 2, CZ-180 00, Praha 8, Czech Republic
[31]NIKHEF, Postbus 41882, NL-1009 DB Amsterdam, The Netherlands
[32]National Technical University, Physics Department, Zografou Campus, GR-15773 Athens, Greece
[33]Physics Department, University of Oslo, Blindern, NO-0316 Oslo, Norway
[34]Dpto. Fisica, Univ. Oviedo, Avda. Calvo Sotelo s/n, ES-33007 Oviedo, Spain
[35]Department of Physics, University of Oxford, Keble Road, Oxford OX1 3RH, UK
[36]Dipartimento di Fisica, Università di Padova and INFN, Via Marzolo 8, IT-35131 Padua, Italy
[37]Rutherford Appleton Laboratory, Chilton, Didcot OX11 OQX, UK
[38]Dipartimento di Fisica, Università di Roma II and INFN, Tor Vergata, IT-00173 Rome, Italy
[39]Dipartimento di Fisica, Università di Roma III and INFN, Via della Vasca Navale 84, IT-00146 Rome, Italy
[40]DAPNIA/Service de Physique des Particules, CEA-Saclay, FR-91191 Gif-sur-Yvette Cedex, France
[41]Instituto de Fisica de Cantabria (CSIC-UC), Avda. los Castros s/n, ES-39006 Santander, Spain
[42]Inst. for High Energy Physics, Serpukov P.O. Box 35, Protvino, (Moscow Region), Russian Federation
[43]J. Stefan Institute, Jamova 39, SI-1000 Ljubljana, Slovenia and Laboratory for Astroparticle Physics,
Nova Gorica Polytechnic, Kostanjeviska 16a, SI-5000 Nova Gorica, Slovenia,
and Department of Physics, University of Ljubljana, SI-1000 Ljubljana, Slovenia
[44]Fysikum, Stockholm University, Box 6730, SE-113 85 Stockholm, Sweden
[45]Dipartimento di Fisica Sperimentale, Università di Torino and INFN, Via P. Giuria 1, IT-10125 Turin, Italy
[46]INFN,Sezione di Torino, and Dipartimento di Fisica Teorica, Università di Torino, Via P. Giuria 1,
IT-10125 Turin, Italy
[47]Dipartimento di Fisica, Università di Trieste and INFN, Via A. Valerio 2, IT-34127 Trieste, Italy
and Istituto di Fisica, Università di Udine, IT-33100 Udine, Italy
[48]Univ. Federal do Rio de Janeiro, C.P. 68528 Cidade Univ., Ilha do Fundão BR-21945-970 Rio de Janeiro, Brazil
[49]Department of Radiation Sciences, University of Uppsala, P.O. Box 535, SE-751 21 Uppsala, Sweden
[50]IFIC, Valencia-CSIC, and D.F.A.M.N., U. de Valencia, Avda. Dr. Moliner 50, ES-46100 Burjassot (Valencia), Spain
[51]Institut für Hochenergiephysik, Österr. Akad. d. Wissensch., Nikolsdorfergasse 18, AT-1050 Vienna, Austria
[52]Inst. Nuclear Studies and University of Warsaw, Ul. Hoza 69, PL-00681 Warsaw, Poland
[53]Fachbereich Physik, University of Wuppertal, Postfach 100 127, DE-42097 Wuppertal, Germany

1 Introduction

As is well known, the Standard Model of electroweak interactions describes the available data with considerable accuracy, only lacking evidence for the Higgs boson as confirmation of its scalar sector [1].

A number of extensions to the scalar sector of the Standard Model allow the current level of agreement between prediction and measurement to be preserved. Beyond the simplest one-doublet scalar sector of the Standard Model, any model with arbitrary numbers of Higgs doublets and singlets will satisfy the above conditions, in particular concerning the relation between the electroweak gauge boson masses and the SU(2)×U(1) mixing angle. To satisfy the constraint given by the apparent weakness of flavour-changing neutral currents, it is generally imposed in addition that every fermion couples to at most one Higgs doublet [2].

Within this framework, the simplest extensions of the Standard Model are the so-called Two-Higgs Doublet Models (2HDM), of which various types exist, depending on the choice of the scalar couplings to fermions. The first type assumes that one doublet only couples to fermions while the other one couples to gauge bosons. At LEP2, the resulting final states include decays of the lightest Higgs boson into photon pairs, which are studied in [3]. The second and most studied type assumes that one doublet couples to the up-type fermions (neutrinos and the u, c, t quarks) while the other one couples to down-type fermions (charged leptons and the d, s and b quarks). Depending on the mixing of the two doublets, the dominant decays of the lightest Higgs boson will be either c quarks and/or gluons (these final states are searched for in [4]), or b quarks and τ leptons. This last case is the focus of this work.

There is a third possible choice of couplings, in which one Higgs doublet couples to leptons only, while the other couples to quarks. In this case, the dominant Higgs boson decay modes may be leptonic, leading, when Higgs bosons are produced in pairs or radiated off primary τ leptons, to the striking four-τ final state.

This paper presents searches for final states occurring in the scenarios decribed above, when Higgs bosons are produced through the Yukawa process, in pairs, or in association with Z bosons. The first section of this work introduces our conventions, describes the data sets and some aspects common to all analyses. Section 2 describes searches for the Yukawa process in LEP1 data; the four-b, four-τ, and $\mathrm{b\bar{b}}\tau^+\tau^-$ final states are addressed. The searches for final states with at least four b quarks or τ leptons at LEP2 are described in Section 3. In all final states, the Higgs boson mass domain is explored from threshold to the kinematic limit. Our results are summarized in Section 4, and include a reinterpretation of the DELPHI Standard Model Higgs boson search [5], constraining the hZ process, when h decays into b quark or τ lepton pairs. Section 5 concludes the paper.

Neutral Higgs bosons beyond the Standard Model have also been searched for by the other LEP Collaborations [6]. The present paper considers additional final states (i.e. the four-τ final state, in Higgs boson pair production and in the Yukawa process), and revisits more usual final states by extending the searched mass range.

1.1 Signals considered in this paper

The extension of the Standard Model Higgs sector by at least one doublet significantly enriches its phenomenology. The Higgs boson spectrum consists of a number of CP-even Higgs bosons (denoted h), CP-odd Higgs bosons (A) and pairs of charged scalars $\mathrm{H}^{\pm}$.

Neutral Higgs boson production mechanisms at LEP are the Bjorken process ($e^+e^-\to hZ$), pair production ($e^+e^-\to hA$) and Yukawa radiation off heavy fermions ($e^+e^-\to f\bar{f}h$ and $e^+e^-\to f\bar{f}A$). The cross-sections of the first two, gauge-mediated processes are (up to kinematic factors) bounded by the Standard Model hZ cross-section; mixing of Higgs doublets induces partial or total suppression with respect to this reference. The third, fermion-mediated process can be significantly enhanced compared to the Standard Model $f\bar{f}h$ cross-section, which is too low to be observed at LEP. Diagrams of these processes are displayed in Figure 1.

Depending on their mass hierarchy, there are a number of production and decay chains involving Higgs bosons (see also Figure 2):

1. $e^+e^-\to hA\to(AA)A$ and $e^+e^-\to hZ\to(AA)Z$ when $m_h > 2\ m_A$;
2. $e^+e^-\to hA\to(AZ)A$ and $e^+e^-\to hZ\to(AZ)Z$ when $m_h > m_Z + m_A$;
3. $e^+e^-\to hA\to h(hZ)$ when $m_A > m_Z + m_h$.

Among these, only processes 1 and 3 are explicitly studied here. Note however that the h(hZ) and the (AZ)A processes involve exactly the same vertices, which means that all distributions are expected to be similar if m_h and m_A are exchanged; as a consequence, our h(hZ) results will be directly translated to the (AZ)A case with swapped h and A masses. On the other hand, the (AZ)Z process is of very small relevance to LEP, since given the available centre-of-mass energies and the presence of two Z bosons in the final states, the open mass domain for h and A is very small.

We limit our analysis to decays of the lighter Higgs boson into b quarks or τ leptons, and only the dominant hadronic Z decays are considered. We take the threshold of Higgs boson decays to b quarks to be 12 GeV/c^2, which slightly exceeds twice the mass of the lightest B mesons. If, due to strong interaction corrections, this threshold appears to be higher, it is enough to truncate our results at the relevant Higgs boson mass values.

Further details of the phenomenology (explicit expressions for production rates and branching fractions) are model dependent (see for example [7] for descriptions). It is however important to note that extensions of the Higgs sector beyond two doublets do not increase the list of available final states. We therefore choose the universal approach to extract, for each process and as a function of the Higgs boson masses, upper bounds on the production cross-section times the branching fraction into the considered final state. These bounds will be expressed in terms of reference cross-sections, defined below for the three primary processes.

Any final state initiated by $e^+e^-\to hZ$ is conveniently expressed in terms of the Standard Model hZ cross-section (we use the computation from [8]) and suppression factors arising from mixing of the Higgs doublets and branching fractions (hereafter denoted R and BR, respectively). Given what is said above, we have:

$$\begin{aligned}
\sigma_{hZ\to b\bar{b}Z} &= \sigma^{SM}_{hZ}\times R_{hZ}\times BR(h\to b\bar{b})\\
&\equiv \sigma^{SM}_{hZ}\times C^2_{Z(h\to bb)};\\
\sigma_{hZ\to\tau^+\tau^-Z} &= \sigma^{SM}_{hZ}\times R_{hZ}\times BR(h\to\tau^+\tau^-)\\
&\equiv \sigma^{SM}_{hZ}\times C^2_{Z(h\to\tau\tau)};\\
\sigma_{(AA)Z\to 4b+jets} &= \sigma^{SM}_{hZ}\times BR(Z\to hadrons)\times R_{hZ}\times BR(h\to AA)\times BR^{\,2}(A\to b\bar{b})\\
&\equiv \sigma^{SM}_{hZ}\times BR(Z\to hadrons)\times C^2_{Z(AA\to 4b)}.
\end{aligned}$$

In the particular case of the 2HDM of type II, characterized by two mixing angles α, β and the two Higgs doublets coupling to the up- and down-type fermions respectively, we would

have $R_{hZ} = \sin^2(\alpha-\beta)$, $\Gamma(h \to b\bar{b}, \tau^+\tau^-) \propto |\sin\alpha/\cos\beta|^2$, and $\Gamma(A \to b\bar{b}) \propto \tan^2\beta$. The factorization of the cross-section into a reference cross-section and a term C^2 containing all details about the Higgs sector is general. Our results will be expressed in terms of $C^2_{Z(h\to bb)}$, $C^2_{Z(h\to\tau\tau)}$, and $C^2_{Z(AA\to 4b)}$[1].

The reference cross-section for $e^+e^-\to hA$ is obtained by computing this process in the absence of any mixing in the Higgs sector (using `HZHA` [9]), and depends only on electroweak constants and the h and A Higgs boson masses. It is thus well-suited to express our results in a general way. The processes that interest us are:

$$\begin{aligned}
\sigma_{hA\to 4f} &= \sigma^{ref}_{hA} \times R_{hA} \times BR(h \to f\bar{f}) \times BR(A \to f\bar{f}) \\
&\equiv \sigma^{ref}_{hA} \times C^2_{hA\to 4f}; \\
\sigma_{(AA)A\to 6b} &= \sigma^{ref}_{hA} \times R_{hA} \times BR(h \to AA) \times BR^3(A \to b\bar{b}) \\
&\equiv \sigma^{ref}_{hA} \times C^2_{hA\to 6b}; \\
\sigma_{h(hZ)\to 4b+jets} &= \sigma^{ref}_{hA} \times R_{hA} \times BR(A \to hZ) \times BR^2(h \to b\bar{b}) \times BR(Z \to hadrons) \\
&\equiv \sigma^{ref}_{hA} \times BR(Z \to hadrons) \times C^2_{Z(hh\to 4b)};
\end{aligned}$$

where f stands for b or τ. In the 2HDM, we would have $R_{hA} = \cos^2(\alpha-\beta)$. Our upper bounds will be set on $C^2_{hA\to 4b}$, $C^2_{hA\to 4\tau}$, $C^2_{hA\to 6b}$, and $C^2_{Z(hh\to 4b)}$.

Reference cross-sections for the Yukawa process are obtained in a similar way. The Standard Model $e^+e^-\to f\bar{f}h$ (f=b,τ) cross-section is used for h production. Computing this cross-section with a suitable (pseudo-scalar) $f\bar{f}A$ vertex gives the reference for A production (both cross-sections are taken from [10]). We obtain:

$$\begin{aligned}
\sigma_{b\bar{b}h\to 4b} &= \sigma^{SM}_{b\bar{b}h} \times R_{b\bar{b}h} \times BR(h \to b\bar{b}) \\
&\equiv \sigma^{SM}_{b\bar{b}h} \times C^2_{bb(h\to bb)}; \\
\sigma_{b\bar{b}h\to b\bar{b}\tau^+\tau^-} &= \sigma^{SM}_{b\bar{b}h} \times R_{b\bar{b}h} \times BR(h \to \tau^+\tau^-) \\
&\equiv \sigma^{SM}_{b\bar{b}h} \times C^2_{bb(h\to\tau\tau)}; \\
\sigma_{\tau^+\tau^-h\to 4\tau} &= \sigma^{SM}_{\tau^+\tau^-h} \times R_{\tau^+\tau^-h} \times BR(h \to \tau^+\tau^-) \\
&\equiv \sigma^{SM}_{\tau^+\tau^-h} \times C^2_{\tau\tau(h\to\tau\tau)};
\end{aligned}$$

and similar expressions for Yukawa production of A bosons. Again $C^2_{bb(h\to bb)}$, $C^2_{bb(h\to\tau\tau)}$, $C^2_{\tau\tau(h\to\tau\tau)}$ and the similar expressions for A contain all terms specific to the Higgs sector under consideration. In 2HDM(II), the vertex enhancement factors $R_{b\bar{b}h}$ and $R_{b\bar{b}A}$ are $|\sin\alpha/\cos\beta|^2$ and $\tan^2\beta$, respectively. Note that since the Z couples much more strongly to b quarks than to τ leptons, the $b\bar{b}(h,A\to \tau^+\tau^-)$ process always has larger cross-section than the mirror $\tau^+\tau^-(h,A\to b\bar{b})$ process. This last process is not considered.

For the hZ and hA initiated processes, the C^2 factors are always products of rotation matrix elements and branching ratios, and therefore always satisfy $C^2 < 1$. The Yukawa processes may have $C^2 > 1$ as well, as illustrated by the 2HDM(II) example above.

Our results may be interpreted in a large number of models and situations. Results on the decay h→AA can be applied to H→hh as well, provided this last channel is open. In the case of CP violation in the Higgs sector, pair production of the two lightest Higgs bosons h_1 and h_2 is different from the CP-conserving $e^+e^-\to hA$ only by an additional

[1] To keep the notation compact, we drop the distinction between particle and anti-particle in the expressions of the C^2 factors.

form factor that can be absorbed in R_{hA}. Similarly, CP-violating Yukawa production of the lightest Higgs boson, $e^+e^-\to f\bar{f}h_1$, can always be written as a weighted sum of the CP-conserving $f\bar{f}h$ and $f\bar{f}A$ cross-sections [11], and can be bounded from below:

$$\begin{aligned}
\sigma_{f\bar{f}h_1} &= \frac{R^S_{f\bar{f}h_1}}{R_{f\bar{f}h}} \times \sigma_{f\bar{f}h} + \frac{R^P_{f\bar{f}h_1}}{R_{f\bar{f}A}} \times \sigma_{f\bar{f}A} \\
&> \left(\frac{R^S_{f\bar{f}h_1}}{R_{f\bar{f}h}} + \frac{R^P_{f\bar{f}h_1}}{R_{f\bar{f}A}} \right) \times \min(\sigma_{f\bar{f}h}, \sigma_{f\bar{f}A}) \\
&\equiv R_{f\bar{f}h_1} \times \min(\sigma_{f\bar{f}h}, \sigma_{f\bar{f}A}),
\end{aligned}$$

where $R^S_{f\bar{f}h_1}$ and $R^P_{f\bar{f}h_1}$ are scalar and pseudoscalar effective couplings of the lightest Higgs boson to the primary fermion, and $R_{f\bar{f}h}$ and $R_{f\bar{f}A}$ are defined above; therefore, comparing a CP-violating model prediction for $e^+e^-\to f\bar{f}h_1$ (summarized in $R_{f\bar{f}h_1}$, and taking branching fractions into account) to our weakest exclusion among the corresponding $e^+e^-\to f\bar{f}h$ and $f\bar{f}A$ processes always yields a conservative answer.

On the contrary, our results on $e^+e^-\to hZ$ do assume standard quantum numbers for the Higgs boson, as a non-standard Higgs boson parity would imply different polarization of the associated Z particle, and hence different polar angle distributions for the final bosons. The signal selection efficiency is thus affected, and our results in this domain should be used with care.

The results also apply to the production of non-Higgs scalar particles. The cross-sections and the analyses presented here however assume that the produced scalars have negligible width (less than 1 GeV).

1.2 Data samples and simulation

The data used in this analysis amount to 79.4 pb^{-1} collected by DELPHI at LEP1, in 1994 and 1995, and 611.2 pb^{-1} collected at the highest LEP2 energies in the years 1998 to 2000. The subsamples and corresponding centre-of-mass energies are listed in Table 1.

A detailed description of the DELPHI detector layout and performance can be found in [12]. The data analysed in this paper were taken in optimal conditions up to the last period of the year 2000, when DELPHI was affected by the failure of one of the twelve sectors of its main tracking device, the Time Projection Chamber (TPC). The tracking algorithm was adapted, and tracks crossing the flawed region were recovered with the silicon Vertex Detector, the Inner Detector, and the Outer Detector. This modification was fully incorporated in the physics events simulation [5].

Large Monte Carlo samples of background and signal events have been produced using the `PYTHIA` [13], `KK2f` [14], `EXCALIBUR` [15], `WPHACT` [16] and `HZHA` event generators. The size of the two-quark (QCD) and four-fermion Standard Model background samples represent about 50 times the luminosity collected at LEP2, and two to five times the luminosity collected at LEP1.

Yukawa events were simulated on the Z resonance with a generator based on [10]. The h and A bosons were radiated off primary τ leptons and b quarks, and decayed into τ lepton or b quark pairs. The signal samples contain 10000 events each, with Higgs boson mass values ranging from threshold up to 50 GeV/c^2.

The available indirect Higgs boson decay channels were simulated for the LEP2 analyses. $(AA)A\to 6b$ events were simulated with m_A between 12 and 50 GeV/c^2 and m_h between 30 and 170 GeV/c^2; $(AA)Z\to(4b)q\bar{q}$ events were simulated with m_A between

Table 1: Centre-of-mass energies and corresponding luminosities used in the analysis. The first and second number for the year 2000 correspond to the luminosity recorded before and after the failure of one TPC sector, respectively.

year	1998	1999				2000
$\sqrt{s}$ (GeV)	189	192	196	200	202	202 to 208
$\mathcal{L}$ (pb^{-1})	158.0	25.9	76.9	84.2	41.1	$164.1 + 61.0$

12 and 50 GeV/c^2 and m_h between 30 and 105 GeV/c^2; h(hZ)$\rightarrow b\bar{b}(b\bar{b}q\bar{q})$ events were simulated with m_h between 12 and 30 GeV/c^2 and m_A from 110 to 170 GeV/c^2. The direct decay processes hA$\rightarrow 4\tau$ and hA$\rightarrow$4b were simulated over the whole kinematically allowed mass range.

The LEP2 background events were simulated at all centre-of-mass energies listed in Table 1. The LEP2 signal events were generated at $\sqrt{s}$ =200 GeV, in mass steps of 5 GeV/c^2 close to the decay thresholds, and 10 GeV/c^2 elsewhere. Dedicated samples for systematic uncertainty evaluation were generated at all LEP2 centre-of-mass energies, for a reduced number of mass points. All LEP2 signal samples contain 2000 events.

All generated events used `PYTHIA` for decay and hadronization and were processed through the detailed DELPHI simulation program [17].

1.3 Methods common to all analyses

Unless stated otherwise, charged particles are selected if their momentum is greater than 100 MeV/c, and if their measured distance to the interaction point is less than 4 cm in the transverse plane, and less than 4 cm/$\sin\theta$ along the beam direction, where θ is the particle polar angle. Neutral particles are defined as calorimetric clusters not associated to tracks, and are selected if their measured energy is larger than 200 MeV in the electromagnetic calorimeter, or larger than 300 MeV in the hadron calorimeter.

The analyses described below select τ particles, and the selection criteria rely partly on the identification of their leptonic decay products. Muons are identified in the muon chambers, where signals coincide with the extrapolation of tracks measured in the central detectors. Muons are also characterized by energy deposits in the hadron calorimeter, compatible with minimum-ionizing particles. Electrons are identified mainly by energy loss measurements in the TPC, shower profile variables in the electromagnetic calorimeter, and by comparing the measured track momentum and associated calorimeter energy. In the analyses searching for τ's at LEP1, the DELPHI standard identification tag is used for both lepton flavours, with performances given in [12]. In the four-τ search at LEP2, the lepton selections are very similar to those developed for the analysis of fully leptonic W pair decays [18].

The method used to select b quark jets is described in detail in [19]. Variables that discriminate between fragmented b quarks (leading to long lived B hadrons) and ordinary jets are combined into a single variable, hereafter denoted x_b for events and x_{bi} for the jet of i-th largest b-likeness (in four-jet events, x_{b1} is the highest jet b-tagging value, and x_{b4} is the lowest). Contributions to this variable are the compatibility of tracks with the primary vertex, based on their measured impact parameter; the transverse momentum of identified leptons with respect to the jet axis; and the rapidity, effective mass, and fraction of the jet momentum, of particles assigned to a possible reconstructed secondary vertex.

All search results presented in this work are interpreted using a modified frequentist technique based on the extended likelihood ratio [20]. For a given experiment, the test statistic Q is defined as the likelihood ratio of the signal+background hypothesis ($s+b$) to the background hypothesis (b), computed from the number of observed and expected events in both hypotheses. Individual events may also carry a signal-to-background ratio based on a measured discriminating variable, such as the reconstructed mass (this possibility is used in the LEP2 four-τ search). Probability density functions (PDFs) for Q in the b and $s+b$ hypotheses are built using Monte Carlo sampling of the (Poisson-distributed) background and signal expectations, and of the optional discriminating variable distributions. The confidence levels CL_b and CL_{s+b} are defined as the integrals of the b and $s+b$ PDFs for Q between $-\infty$ and the actually observed value Q_{obs}. The confidence level in the signal hypothesis, CL_s, is conservatively approximated by the ratio CL_{s+b}/CL_b. 1-CL_s measures the confidence with which the signal hypothesis can be rejected, and will be larger than 0.95 for an exclusion confidence of 95%.

2 LEP1 data analysis

This section describes the search for the Yukawa process in LEP1 Data. The four-b, $b\bar{b}\tau^+\tau^-$, and four-τ final states are analysed.

2.1 The four-b final state

This section describes a search for neutral Higgs boson production in the four-b channel. The analysis is focused on the Yukawa process, and subsequently applied to Higgs boson pair production.

Let us first discuss the issue of the background estimation. An irreducible background contribution originates from events with two primary b quarks and a gluon splitting into a second b quark pair, i.e. $Z \to b\bar{b}(g \to b\bar{b})$. This gluon splitting happens with a probability g_{bb}. The most recent theoretical estimate is $g_{bb}^{th} = 1.75 \pm 0.40 \times 10^{-3}$ [21]. In the simulation we use $g_{bb} = 1.5 \times 10^{-3}$, the default value in [13], somewhat below the theoretically preferred value. This quantity has also been measured by the LEP and SLD Collaborations, with an average result of $g_{bb}^{exp} = 2.74 \pm 0.42 \times 10^{-3}$ [22].

The available measurements are however not insensitive to four-jet events with light Higgs boson decays to b quark pairs which, if present, would contaminate the selected samples and lead to an overestimation of the measured g_{bb} value. This possibility was not taken into account in [22]. The efficiency of these analyses on Higgs boson events has not been estimated, and therefore the g_{bb} measurements potentially contain a contribution from Higgs boson events.

Our strategy is therefore to keep the value of $g_{bb} = 1.5 \times 10^{-3}$ in the simulation. The possible presence of an excess in the data can then be interpreted in two alternative ways: either by attributing the excess to gluon splitting events and estimate the additional contribution to g_{bb} (this is not the focus of this paper, and will be done only indicatively in the following), or by attributing the excess to the signal and obtain conservative limits on Higgs boson production. Considering the large uncertainties on the various estimates of g_{bb}, we do not use this channel for signal discovery.

The analysis itself is described in the following. For Higgs boson masses of about half of the Z mass we expect a four-jet topology, whereas close to threshold only three jets may be reconstructed. Taking this into account we develop two parallel selection procedures, corresponding to event reconstructions in three and four jets respectively.

Table 2: Number of observed and expected background events in the Yukawa four-b analyses, at various steps of the selection; $g_{bb} = 1.5 \times 10^{-3}$.

Cut			Total background	Data (94-95)
preselection			141128 ± 207	142527
three-jet topology:		$x_{b3} > -2$	140705 ± 206	142042
	Bin 1	$1.5 > x_{b3} > 1.25$	2.2 ± 0.9	5
	Bin 2	$x_{b3} > 1.5$	3.2 ± 1.1	5
four-jet topology:		$x_{b34} > -2$	11421 ± 17	11848
	Bin 1	$1.0 > x_{b34} > 0.5$	3.4 ± 1.1	7
	Bin 2	$x_{b34} > 1.0$	3.5 ± 1.0	4

At first, the events are required to contain at least six charged particles. At this preselection stage we force the reconstruction of three jets, and the 2→3 jet transition point y_{23} of the Durham algorithm [23] should be greater than 0.01. For all reconstructed jets, the b-tagging values x_{bi} are computed as described in Section 1.3, and ordered from higher to lower b-likeness. The b-tagging variable of the most b-tagged jet, x_{b1}, is required to be greater than 0.

The preselection eliminates all backgrounds but hadronic Z decays. Non-b hadronic events are significantly reduced as well and represent about 10% of the remaining sample. After this step, all events are reconstructed as four-jet events.

The remaining b-tagging discriminating power is contained in the least tagged jets. The final selection relies on x_{b3} in the three-jet topology, and on the sum $x_{b34} = x_{b3} + x_{b4}$ in the four-jet topology. The distributions of these variables are shown in Figure 3. In both the three-jet and four-jet analyses, two channels are defined for the final analysis (denoted Bin 1 and Bin 2, see again Figure 3). They are chosen to have a similar expected background, and a signal efficiency of at least 1% to 2% in Bin 2.

Numerical comparisons between the data and the simulation are shown in Table 2. The 1% difference seen at the preselection level is explained by residual imperfections of the b-tagging efficiency simulation [19]. At the end of the analysis, an excess of data is observed in all channels. One explanation could be the possible underestimation of the gluon splitting probability.

Efficiencies for h and A production in the Yukawa process are shown in Table 13. For the interpretation of results, the three-jet or four-jet analysis is chosen at each mass point as a function of the expected exclusion performance.

The selection developed for this search is directly applied to pair production of neutral Higgs bosons, with efficiencies given in Table 14. The efficiencies are evaluated for both three-jet and four-jet analyses, and found to be almost always better in the second case. The four-jet analysis is retained for the interpretation of the results, described in Section 4.2.

The systematic uncertainty related to the residual differences between b-tagging efficiency in data and in the simulation is estimated using Ref. [19], where it is shown that the difference is limited to ±10% for high purity b jet selection. This uncertainty is assumed, and added in quadrature to the statistical uncertainty from the limited size of the simulation samples. Considering the conservative assumptions on data and background described above, no further systematic uncertainty is assumed.

A fit to the $b\bar{b}$ and $b\bar{b}g$→4b components of the data is performed as a cross-check. An independent sample of four-b events with gluon splitting is introduced, and its normal-

ization is adjusted so that its addition to the standard simulation (with $g_{bb} = 1.5 \times 10^{-3}$) reproduces the observation. In the three-jet analysis, the additional contribution is found to be $(3.0 \pm 0.7) \times 10^{-3}$, bringing the total gluon splitting value to $(4.5 \pm 0.7) \times 10^{-3}$. In the four-jet analysis, $(3.2 \pm 0.7) \times 10^{-3}$ is found, leading to a total of $(4.7 \pm 0.7) \times 10^{-3}$. The result is displayed in Figure 3 as well. This estimation of g_{bb} is purely indicative.

2.2 The $b\bar{b}\tau^+\tau^-$ final state

In the $b\bar{b}\tau^+\tau^-$ final state of the Yukawa process (i.e., $b\bar{b}(h\to\tau^+\tau^-)$), the Higgs boson decay products often have high momentum, and appear as a collimated slim jet. We therefore reconstruct three jets in this final state, of which one is expected to contain a pair of τ leptons of low decay multiplicity. The two other jets, initiated by b quarks, are expected to have higher multiplicity.

As in the previous analysis, event reconstruction is forced into three jets using the Durham algorithm. The b-tagging algorithm is then applied to evaluate the b-likeness at both the event and jet levels. The jets are ordered according to their b-tagging value; the two jets with highest value are assumed to be b-jets.

At the preselection level we require the total charged multiplicity in the event to be at least 10. As before, the Durham parameter y_{23} is required to be greater than 0.01. The event b-tagging variable x_b must be greater than 0. The cosine of the angle between the two b-jets should satisfy $\cos\alpha_{12} < 0.9$. The preselection eliminates almost all non-hadronic background components, leaving mostly $Z\to b\bar{b}$ events.

Furthermore, x_{b1} is required to be greater than 0 and x_{b2} to be greater than -1. The jet with lowest b-tagging value is supposed to correspond to the τ pair. Events with gluon radiation may fake the signal, but gluon jets usually have high multiplicity, whereas we expect the τ pair to be narrow and have low multiplicity. For the remaining cuts, only charged particles of momentum greater than 1 GeV/c are taken into account.

The jet of lowest b-likeness is required to have a charged multiplicity of 1, 2 or 3, and a total multiplicity of at least 2. Its broadness, defined as the cosine of the largest angle between two particles in the jet, $|\cos\theta|$, should be larger than 0.64. The sum of momentum fractions of the two particles with the highest momentum in this jet, denoted $(p_1 + p_2)/E_3$ (where E_3 is the energy of the jet of lowest b-likeness), should be greater than 0.5. Furthermore, we require at least one leptonic τ decay, by demanding an identified lepton (muon or electron), with p_T >1 GeV/c (where p_T is defined as the transverse momentum of the lepton with respect to the jet axis). Figure 4 illustrates three of the selection variables described above.

Seven events are selected in the data, whereas 10.6±2.3 events are expected from background processes. Along the whole selection procedure, hadronic Z decays are the dominant background contribution; less than 5% arise from four-fermion processes. Numerical comparisons between data and simulation are shown in Table 3.

The selection efficiencies for $b\bar{b}(h\to\tau^+\tau^-)$ and $b\bar{b}(A\to\tau^+\tau^-)$ are given in Table 15. The small difference in rejection between data and expected background, evaluated at the preselection level and for each selection variable, leads to a systematic uncertainty of 3.0% on the background expectation, and to 3.8% on the signal efficiency. These values are added in quadrature to the statistical errors given in Tables 3 and 15.

Table 3: Number of observed and expected background events in the Yukawa $b\bar{b}\tau^+\tau^-$ analysis, at various steps of the selection.

Cut	Total background	Data (94-95)
preselection	120015 ± 285	116485
x_{b1}, x_{b2}	38385 ± 161	36195
3^{rd} jet multiplicity	10015 ± 83	9808
3^{rd} jet broadness	2143 ± 38	2033
lepton ID	461.9 ± 17.9	430
lepton p_T	10.6 ± 2.3	7

2.3 The four-τ final state

In this section we describe a search for Higgs boson production in the four-τ channel, via the Yukawa process. This final state can be dominant in models where Higgs doublets couple preferentially to leptons. Since the one-prong τ decay is largely dominant, a first analysis, sensitive to events with four charged particles seen in the detector, is described below. Nevertheless, when four τ's are present, the probability that one of them decays into three charged particles is significant. To account for these events, a complementary analysis is developed and is described in the second part of this section. These four-prong and six-prong decays represent respectively 53.1% and 37.8% of all events with four τ leptons.

Due to the nature of the final states considered here (i.e., low multiplicity and low visible energy) the acceptance criteria for reconstructed particles are tightened compared to the description given in Section 1.3. Charged particles are now selected if their momentum is larger than 400 MeV/c, their angle with respect to the beam axis is larger than 20°, they are seen in the TPC and finally, their impact parameter along the beam axis is less than 3 cm.

2.3.1 The four-prong selection

The following series of preselection cuts are used to reject events from beam-gas interactions and from $\gamma\gamma$ collisions. Only events with exactly four reconstructed charged particles are considered. The total electric charge of the particles must be 0. The sum of the impact parameters with respect to the beam-spot must be less than 300 μm in the transverse plane. The pair of oppositely charged particles of lowest invariant mass, denoted $m_\pm$ in the remaining of this section, must be separated from at least one of the remaining charged particles by more than 90°. The invariant mass $m_\pm$ must be larger than 200 MeV/c^2. The missing momentum along the beam axis must be less than $35\%\sqrt{s}$. Finally, either the missing transverse momentum must be larger than $5\%\sqrt{s}$, or the visible mass must be greater than 25 GeV/c^2.

At this stage, the main background consists of $Z\to\tau^+\tau^-$ events, where the τ's have decayed into one prong and three prongs, respectively. This background is reduced by requiring the lowest triplet invariant mass to be greater than 2 GeV/c^2. The remaining $\tau^+\tau^-$ events have both τ's decayed into three prongs, when one charged particle is missed in each hemisphere. To reject them, the visible mass recoiling against $m_\pm$ is required to be larger than 2 GeV/c^2.

Remaining backgrounds come from low-multiplicity hadronic Z decays and four-fermion events. These background components are reduced by requiring the pair of

charged particles recoiling against $m_{\pm}$ to have a mass larger than 10% of the total visible mass. Furthermore, the neutral multiplicity must not exceed six. Four-fermion events not containing τ leptons are rejected by requiring the visible mass to be less than 60 GeV/c^2. One of the particles in $m_{\pm}$ should be identified as an electron or muon, and the other one should not be identified as a lepton of the same flavour; the remaining two charged particles should not both be identified as electrons or muons. Finally, the cut on the invariant mass $m_{\pm}$ is tightened to $m_{\pm}$ >1 GeV/c^2.

Distributions of the visible mass and of the lowest triplet mass are displayed in Figure 5 at the preselection level. The distribution of the $m_{\pm}$ invariant mass is also shown, just before the last cut is applied, with seven observed events and 10.8±1.0 expected events.

After all selection cuts are applied, four events are observed in the data, while 4.1±0.5 are expected from background, all of which are genuine four-fermion events; the contribution from four-lepton events with at least one τ pair amounts to 3.8±0.5 events and the remaining originates from four-lepton events with electrons and muons only.

Comparisons between data and simulated background samples are shown in Table 4. Signal efficiencies vary from 3% to 6%, going from low to high signal mass (see Table 16 for details). These efficiencies correspond to 5.7% and 11.8% of the true four-prong decays of the signal.

2.3.2 The six-prong selection

Exactly six reconstructed charged particles are required in this search. The remaining preselection criteria against beam-gas and $\gamma\gamma$ events are applied as above.

Since one of the τ leptons is expected to decay in the three-prong mode, the lowest triplet invariant mass should not exceed m_τ; the cut is applied at 1.8 GeV/c^2. Moreover, this triplet is required to have momentum larger than 3 GeV/c. It is then treated as a pseudo-particle, and the six-prong topology becomes a pseudo-four-prong one.

To reject low multiplicity hadronic Z decays and τ pair decays into six prongs, the system recoiling against the triplet of lowest mass should have a mass greater than 4 GeV/c^2, and the total multiplicity must be less than 13. The visible mass is required to be less than 60 GeV/c^2. The pair of oppositely charged particles of lowest invariant mass must pass the cut $m_{\pm}$ >1 GeV/c^2 (here, the pair may contain the pseudo-particle made by the triplet of lowest invariant mass).

Distributions of the minimal triplet mass, and of the mass of the three charged particles recoiling against it, are displayed at the preselection level in Figure 6. The distribution of the invariant mass $m_{\pm}$ is also shown, just before the final cut is applied. At this level, 13 events are observed and 14.2±2.9 are expected.

After all cuts, four events are observed, while 6.0±1.5 are expected from the simulation. Of these, 3.4±1.4 are hadronic Z decays, 1.9±0.2 are four-lepton events with at least one τ pair. The remaining contribution comes from four-fermion events with two quarks and two leptons.

The cut-by-cut evolution of the data and simulated background samples is shown in Table 5. Signal efficiencies vary from 2.5% at low mass, to 5.6% at high mass, corresponding to 6.3% to 14.9% of the true six-prong decays of the signal. Details can be found in Table 17.

Systematic uncertainties on the expected backgrounds and on the signal efficiencies are estimated as in Section 2.2. Each selection cut described above is applied in turn at the preselection level, and the difference in rejection between the data and the simulation

is attributed to the imperfect modelling of the corresponding distribution. The resulting uncertainties amount to 8% on backgrounds and 5% on signals in the four-prong analysis, and to 3.5% on backgrounds, and 3% on signals in the six-prong analysis.

Table 4: Four-τ final state at LEP1. Number of observed and expected background events, at various stages of the four-prong analysis.

Cut	$\tau^+\tau^-$	$q\bar{q}$	4f	Total	Data (94-95)
preselection	10586.0	1148.1	177.3	11911.4±168.5	11876
anti-$\tau^+\tau^-$	8.7	444.3	152.1	605.1± 17.7	574
anti-$q\bar{q}$	3.3	20.8	121.7	145.8± 6.7	137
final selection			4.1	4.1± 0.5	4

Table 5: Four-τ final state at LEP1. Number of observed and expected background events, at various stages of the six-prong analysis.

Cut	$\tau^+\tau^-$	$q\bar{q}$	4f	Total	Data (94-95)
preselection	935.1	5744.4	80.5	6760.0±84.8	6733
anti-$\tau^+\tau^-$, $q\bar{q}$	4.3	52.3	5.2	61.8±11.7	58
final selection		3.4	2.6	6.0± 1.5	4

3 LEP2 data analysis

The searches for final states with at least four b quarks or with exactly four τ leptons in LEP2 data are described in what follows.

3.1 Final states with b quarks

This section describes a search for cascade decays of neutral Higgs bosons. The considered decay chains are hA$\rightarrow$(AA)A, hZ$\rightarrow$(AA)Z, hA$\rightarrow$(AZ)A and hA$\rightarrow$h(hZ). The lightest Higgs boson is assumed to decay into b quark pairs. The final state will contain six quarks, of which at least four are b quarks. The analysis developed here is also applied to the direct decay hA$\rightarrow$4b.

Events with cascade decays a priori lead to a six-jet final state. However, when the mass of the lighter Higgs boson approaches $2m_b$, the decay jets may not be resolved. This then leads to a three-jet topology in the (AA)A channel, or to a four-jet topology in the (AA)Z or h(hZ) channels.

Due to the large range of masses and topologies that are searched for, different signals often differ more among themselves than from the background. Instead of analysing each topology individually, we have designed a polyvalent method exploiting only the presence of at least four b quarks.

The preselection used in this analysis has been developed for Standard Model Higgs boson searches in hadronic events [5], and is briefly outlined here. Multiplicity and energy flow cuts eliminate radiative and $\gamma\gamma$ events, and significantly reduce the QCD background. Selected events are then forced into a four-jet configuration using the Durham algorithm, and the mass of each jet is required to exceed $1.5\,\mathrm{GeV/c^2}$.

The rest of the analysis does not rely on event shapes, and uses only b-tagging information. Variables with large discriminating power are the secondary vertex multiplicity N_{vg}, the b-likeness variables x_{b1} and x_{b2}, and the b-likeness sum $x_{b34} = x_{b3} + x_{b4}$. Considering the total number of secondary vertex hypotheses N_v, which includes secondary vertices failing the fit-quality selection (see [19]), achieves supplementary discrimination. A combined variable, denoted B in the following, is defined as the sum of the logical values of the following conditions (each satisfied condition increases the value of B by 1 unit):

$$\mathrm{B} = (N_{vg} > 2) + (N_v > 5) + (x_{b1} > 2) + (x_{b2} > 0) + (x_{b34} > -2).$$

For the final selection, B is required to be greater than 3. A preselection-level data to simulation comparison of the distributions of some analysis variables is shown in Figure 7. Numerical comparisons between the data and the simulation are shown in Tables 6 and 7.

The excess observed in the data of 2000a after the last cut (see Table 7) has been verified to be unrelated to any spurious event reconstruction problem. Its possible meaning will be discussed in Section 4.2. The breakdown of this sample in centre-of-mass energy windows, as shown in Table 8, does not indicate a high mass signal appearing at the highest centre-of-mass energy. The data taken in 1998, 1999, and 2000b, agree with the Standard Model background expectation.

Since the signal samples were generated at only one centre-of-mass energy (namely $\sqrt{s}$ =200 GeV), a procedure is designed to estimate the efficiencies at the other energies. To do so, the four-momenta of the primary bosons are rescaled to correspond to the desired centre-of-mass energy, and all particles coming from the primary pair are boosted accordingly. Rescaled events are analysed using the analysis chain described above. The validity of this procedure was verified using a few dedicated signal samples simulated at the extreme centre-of-mass energies corresponding to the analysed data set, i.e. 189 and 208 GeV. The method proves to have a precision of $\pm 2\%$.

The signal efficiencies for the simulated mass points are given in Tables 18, 19, and 20. The efficiency for any arbitrary mass point is obtained by linear interpolation between the three closest simulated points. The analysis described above is also directly applied to the hA$\rightarrow$4b channel, with resulting efficiencies given in Table 21.

In addition to the uncertainties already quoted, a systematic error is included accounting for residual imperfections in the b-tagging description in the simulation. An uncertainty of $\pm 5\%$ is assumed [19].

Uncertainties on the gluon splitting probability have much smaller impact (as in Section 3.1, we use $\mathrm{g_{bb}} = 1.5 \times 10^{-3}$). Compared to the LEP1 four-b analysis, the present selection needs to preserve high signal efficiency. The background rejection is thus much weaker, and the fraction of events predicted to contain gluon splitting into $\mathrm{b\bar{b}}$ after the last cut is only 2%. Assuming 50% uncertainty on this fraction contributes an uncertainty of 1% on the background estimate.

3.2 The four-τ final state

This final state consists of four narrow jets of low multiplicity coming from the τ decays. When the h or A boson mass decreases, the decay products are often observed as a single jet, due to the low angle between the decay τ leptons. Three independent analysis streams are developed to provide sensitivity to the whole ($\mathrm{m_h}$,$\mathrm{m_A}$) mass plane: a four-jet, a three-jet and a two-jet stream, respectively adapted to the case where both bosons are heavy, one boson is light, or both h and A are light.

Table 6: Final states with b quarks. Comparison between data and simulation at the preselection level. The data sets 2000a and 2000b correspond to data taken before and after the failure of TPC sector 6, respectively.

Data set	4f	$q\bar{q}$	Total	Data
189 GeV	1144.1	739.6	1883.7 ± 28.3	1896
192 GeV	198.3	105.6	303.9 ± 4.2	319
196 GeV	595.1	298.2	893.3 ± 14.3	919
200 GeV	655.2	312.5	967.7 ± 14.5	949
202 GeV	318.2	144.2	462.4 ± 6.9	465
2000a	1295.1	563.1	1858.2 ± 27.9	1826
2000b	447.5	192.0	639.5 ± 9.6	632
all energies	4653.6	2355.2	7008.8 ± 46.4	7006

Table 7: Comparison between data and simulation for events satisfying B > 3 (final selection). The data sets 2000a and 2000b correspond to data taken before and after the failure of TPC sector 6, respectively.

Data set	4f	$q\bar{q}$	Total	Data
189 GeV	1.4	1.6	3.0 ± 0.7	2
192 GeV	0.2	0.5	0.7 ± 0.3	2
196 GeV	1.1	1.0	2.1 ± 0.4	2
200 GeV	1.0	1.0	2.0 ± 0.3	2
202 GeV	0.3	0.5	0.8 ± 0.2	1
2000a	2.1	1.6	3.7 ± 0.6	10
2000b	0.6	0.6	1.2 ± 0.2	1
all energies	6.8	6.9	13.7 ± 1.8	20

Table 8: Breakdown of the excess observed in 2000a, and the corresponding expected background. Three centre-of-mass energy windows are used, namely $\sqrt{s} < 205.5$, $205.5 < \sqrt{s} < 207.1$, and $\sqrt{s} > 207.1$.

Energy window (GeV)	Exp. bg	Data
$\sqrt{s} < 205.5$	1.6 ± 0.3	5
$205.5 < \sqrt{s} < 207.1$	1.9 ± 0.4	4
$\sqrt{s} > 207.1$	0.2 ± 0.1	1

Some criteria are common to all analyses. A charged-particle multiplicity between 4 and 8 is required, to reject lepton pairs and hadronic events. Algorithms used in the lepton identification are the same as those used in the selection of fully-leptonic W pairs [18]. The four-lepton background is rejected by requiring that the momentum of the most energetic identified muon or electron, if present, is less than $0.25\sqrt{s}$. If a second muon or electron is identified, it should have momentum less than $0.15\sqrt{s}$. In the following, jets are defined as clusters of particles (of which at least one is charged) contained in a cone with a 15° opening angle. The analysis streams are now described in turn.

3.2.1 The four-jet stream

The four-jet analysis is derived from that of the four-τ final state applied in the search for doubly charged Higgs bosons (Section 3.1 of Ref. [24]), but discarding all mass cuts. Events are clustered into jets, and each jet is required to be separated from the others by at least 15°. Only events with four reconstructed jets are accepted and every jet is considered as a τ candidate.

To improve the reconstruction of the τ energy, the τ momenta are rescaled, imposing energy and momentum conservation while preserving the measured directions. If any rescaled jet momentum is negative, the event is rejected.

The two-photon background is reduced by the following requirements: the momenta of the jets have to be larger than $0.01\sqrt{s}$, the visible energy outside a cone of 25° around the beam-axis is required to be greater than $0.15\sqrt{s}$, and the total energy of neutral particles should be less than $0.35\sqrt{s}$.

After all cuts only one event is observed in the data, while 1.9 events are expected from background processes. Efficiencies around $40-50\%$ are obtained for h and A masses higher than $\sim$50 GeV/c^2.

The rescaled τ momenta are used to reconstruct the Higgs boson masses after the jets are paired according to their charges and the dijet masses. The charge of a jet is defined as the sum of the charges of the jet particles if this sum is found to be ±1, and as the charge of the most energetic charged particle of the jet otherwise. The pairing is chosen so as to minimise the difference between the two reconstructed dijet masses. After pairing, the sum of the dijet masses is used as a discriminating variable in the confidence level computations (Section 1.3).

3.2.2 The three-jet stream

Events enter this stream if three jets are found after clustering is performed as in the four-jet stream. Each jet is considered as a τ candidate, and should again be separated from the others by at least 15°. To reject the two-photon background, the same criteria as described in Section 3.2.1 are used.

Additional cuts are applied to reduce the remaining $Z\gamma^\star$ background. The absolute value of the cosine of the missing momentum polar angle should be less than 0.9. All jets should have polar angle between 20° and 160°. For signal events, the three reconstructed jets are expected to be in the same plane. Therefore, the sum of the three angles between the jets, α_{123}, is required to be greater than 357°. Finally, the lowest jet-jet angle, α_1, is required to be greater than 25°.

Six events are selected in the data, while 6.5 events are expected from the background. The efficiency for m_A=4 GeV/c^2 and m_h greater than 60 GeV/c^2 is about 40%.

The final discriminating variable for the confidence level computations is the highest reconstructed Higgs boson mass, since the other one is expected to be low. This mass

is calculated by rescaling the momentum of the jets, imposing energy and momentum conservation while keeping the jet directions fixed. The pairing is then chosen as follows. If only one jet has an electric charge equal to 0, the mass is given by the opposite jet pair. In other cases, the mass is given by the two jets, if they exist, containing only one charged particle; or by the two jets with opposite charges, if the third one has an electric charge greater than 1 in absolute value. If none of these configurations is present, the mass is given by the two jets of opposite charges and with nearest rescaled τ momenta.

3.2.3 The two-jet stream

If an event is not classified in the two previous streams, it is a candidate for the two-jet analysis. Only events with either four or six charged particles, and with total electric charge zero, are accepted in this stream.

Every neutral particle energy is added to the momentum of the nearest charged particle, if it is distant by less than 15°. Neutral particles making angles larger than 15° with all charged particles are not recombined.

A charged multiplicity of six signals that one of the τ leptons has decayed into three prongs. To ensure this is the case, the lowest triplet invariant mass should not exceed 1.4 GeV/c^2 and its momentum should be greater than 5 GeV/c.

At this stage, events are grouped into four τ candidates, coming from either the four charged particles, or the three charged particles plus the opposite triplet of lowest mass. The two-photon background is reduced by requiring all τ candidate momenta to be larger than $0.005\sqrt{s}$, and the visible energy outside a cone of 25° around the beam-axis is required to be between $0.15\sqrt{s}$ and $0.8\sqrt{s}$. In addition, events with the third lowest angle between τ candidates, α_3, less than 70° are rejected. Finally, the polar angles of all τ candidates must lie between 25° and 155°, while at least one must have a polar angle between 50° and 130°.

Six events are selected in the data, in agreement with the 9.5 events expected from the background processes. The efficiency for m_A=4 GeV/c^2 and m_h=4 GeV/c^2 is 37%. The mass estimation often fails in this topology, and it is not possible to reconstruct either the h mass or the A mass. The second lowest angle between τ candidates is chosen as final discriminating variable in the confidence level computations.

Good agreement between the data and the expected background is observed for each analysis, as illustrated in Figure 8. Combining all streams, 13 events are selected in the data, whereas 18.0±1.2 events are expected from the Standard Model background processes. Details are shown in Tables 9, 10 and 11. The efficiencies of the four-τ analysis streams are shown in Table 22 for representative simulated mass points.

All results contain statistical and systematic uncertainties added in quadrature. Systematic uncertainties are estimated by varying the simulated charged particle momenta, jet-jet angles and particle identification variables in a range given by the residual differences between their distributions in data and simulation. Because of the large amount of missing energy in this final state, the efficiencies are expected to vary slowly with $\sqrt{s}$. Using a few dedicated signal samples simulated at different centre-of-mass energies corresponding to the analysed data set, this is verified to be true up to ±1.5%. Taking this into account, the total systematic uncertainty amounts to about ±3% for signal efficiencies, and to ±10-13% for the background; these last numbers are dominated by the finite Monte Carlo statistics.

Table 9: Four-τ final state. Number of observed and expected background events, at various stages of the four-jet analysis stream, for the total 189-208 GeV sample.

Cut	four-lepton	others	Total	Data
four-jet preselection	44.0	23.4	67.4	59
anti $\gamma\gamma$	28.9	2.1	31.0	26
anti four-lepton	1.7	0.2	1.9$\pm$0.2	1

Table 10: Four-τ final state. Number of observed and expected background events, at various stages of the three-jet analysis stream, for the total 189-208 GeV sample.

Cut	four-lepton	others	Total	Data
three-jet preselection	39.2	153.4	192.6	199
anti four-lepton	9.6	90.8	100.4	98
anti $\gamma\gamma$	5.9	12.5	18.4	22
α_{123}, α_1 cuts	2.7	3.9	6.6$\pm$0.7	6

Table 11: Four-τ final state. Number of observed and expected background events, at various stages of the two-jet analysis stream, for the total 189-208 GeV sample.

Cut	four-lepton	others	Total	Data
τ selection	31.3	1299.9	1331.2	1358
anti $\gamma\gamma$	14.0	502.4	516.4	517
α_3	3.7	11.8	15.5	13
Jet angular cuts	1.6	7.9	9.5$\pm$1.0	6

4 Results

The results from the analyses described above are summarised in this section. The Yukawa process, hA and hZ production followed by direct Higgs boson decays into fermions, and cascade decays are discussed in turn. The excess found in the LEP2 b-tagging analysis is discussed. Since no obvious signal is found, the observations are interpreted in terms of excluded cross-sections, using the conventions described in Section 1.1. For all final states, the tables given in Appendix B provide explicit numerical upper bounds on the corresponding C or C^2 factors. All the limits presented in the following are at the 95% confidence level (CL).

4.1 Search for the Yukawa process at LEP1

Results of the Yukawa production analyses of Section 2 are presented in the form of mass-dependent upper bounds on the C^2 factors defined in the introduction. Reference cross-sections for Yukawa production of h and A are obtained using [10]. In all cases, the mass range between production threshold and 50 GeV/c^2 is considered, and the C^2 values excluded at exactly 95% CL are determined. Since these values are very large, the numbers given in Table 23 and the corresponding figures refer to C rather than to C^2. The former corresponds to the matrix-element enhancement factor, when 100% branching fraction into the relevant final state is assumed.

The four-b Yukawa results on $C_{bb(h\to bb)}$ and $C_{bb(A\to bb)}$, shown in Figure 9, are obtained by combining Bin 1 and Bin 2 as independent channels, either in the three-jet analysis or in the four-jet analysis, keeping the analysis with the best expected exclusion sensitivity at each mass point. The $b\bar{b}\tau^+\tau^-$ channel leads to the upper bounds on $C_{bb(h\to\tau\tau)}$ and $C_{bb(A\to\tau\tau)}$ displayed in Figure 10. Results on the four-τ channel are shown in Figure 11. Upper bounds are placed on $C_{\tau\tau(h\to\tau\tau)}$ and $C_{\tau\tau(A\to\tau\tau)}$ by combining the independent four-prong and six-prong analyses.

The slight deficit in the $b\bar{b}\tau^+\tau^-$ channel translates into an exclusion slightly stronger than expected. On the contrary, the excess in the four-b channel induces an exclusion which is slightly weaker (at 1σ) than expected from the simulation. The four-τ channel result is in agreement with the background hypothesis.

In the four-b analysis, the inclusion of Bin 1 improves the sensitivity on $C_{bb(h\to bb)}$ by 10%, compared to using Bin 2 alone. In the four-jet analysis, Bin 2 excludes signals larger than 7 events, which could be compared to our previous result [25], where the limit was set at 50.4 events. The improvement in sensitivity on $C_{bb(h\to bb)}$ and $C_{bb(A\to bb)}$ is nearly threefold over the whole mass range. The three-jet analysis has better expected performance than the four-jet analysis in the very low mass region (below m_h,$m_A \sim 15$ GeV/c^2).

As the figures indicate, the four-b and the $b\bar{b}\tau^+\tau^-$ channels have similar intrinsic sensitivity (the expected exclusions are similar). This is not the case for the four-τ channel. Although the signal to background ratio in this channel is better than that in the four-b and $b\bar{b}\tau^+\tau^-$ channels (as can be seen from Tables 4, 5, 16 and 17), the much weaker coupling of the Z boson to the primary τ leptons induces weaker sensitivity on $C_{\tau\tau(h\to\tau\tau)}$ and $C_{\tau\tau(A\to\tau\tau)}$.

Numerical values for the observed exclusions are given in Table 23.

4.2 hA and hZ production: direct decays

Higgs boson production in the hA$\rightarrow$4b and hA$\rightarrow 4\tau$ channels is assessed using the results of the analyses described in Sections 2.1, 3.1 and 3.2, as well as those of the searches for the hA$\rightarrow$4b process in the MSSM framework at all LEP2 energies, as described in Ref. [5]. Exclusion limits are also given for the hZ process when the Higgs boson decays into b quark pairs or τ lepton pairs, using the results of the searches for the hZ process applied to all LEP2 data samples, as described in [5].

The C^2 factor for each process is defined in the introduction. The Higgs boson mass domain is then scanned, and at each point the C^2 value excluded at exactly 95% CL is determined.

Event rates for the hA process are computed with the `HZHA` generator [9], and using interpolation of the signal efficiencies (Tables 21 and 22, Appendix A). Rates for the hZ production process are determined as described in [5]. The combination of data at different centre-of-mass energies is done assuming the expected evolution of the hA and hZ production cross-sections with energy.

4.2.1 The four-b search

Figure 12 shows the results of the search for hA$\rightarrow$4b. The LEP1 data analysis presented in Section 2.1 is combined with the LEP2 analyses of Section 3.1 and of Ref. [5]. As these last two analyses are not independent, only the analysis with the best expected exclusion power is kept at each mass point and at each centre-of-mass energy. While the analysis presented in this paper has good performance over the whole mass plane, the MSSM analysis [5] has optimal sensitivity when $m_h \sim m_A$ and provides better results in this region.

A strong sensitivity is obtained both at high mass from LEP2 data, and in the lower mass region where the LEP1 data contribute significantly. In the case of no suppression (i.e. full strength production, and 100% branching into four b quarks, i.e. $C^2_{hA\rightarrow 4b}=1$), the search excludes a region roughly given by $m_h, m_A > 12$ GeV/c^2, $m_h, m_A < 130$ GeV/c^2 when the opposite mass is small, and $m_h + m_A < 180$ GeV/c^2 when the h and A masses are similar. When the suppression factor is less than 5%, the excluded region is obtained essentially from LEP1 data.

The consistency of the numerical excess found in the data of 2000a, with the data recorded in 1998, 1999, and 2000b, is estimated in the following way. The excess is attributed to a signal, and used to normalize its cross-section. It is then possible to confront the signal hypothesis with the data surviving the selections in the complementary data sets. Given 6.3 signal events in 2000a, the number of signal events expected in the other data sets depends on the nature of the signal and its mass. The primary signal process is taken to be $e^+e^-\rightarrow$hA, since its cross-section rises more slowly with energy than the hZ cross-section. The conclusions made for hA are then a fortiori valid for hZ. Three mass hypotheses are considered, namely $(m_h, m_A)=(90,90)$, (95,95), and (100,100) GeV/c^2. The corresponding rates are summarized in Table 12, correctly taking into account the kinematic thresholds. In each case the confidence levels in the background and signal hypotheses are given.

In all cases, a signal corresponding to the observed excess in 2000a would produce a visible signal in the other data sets. Since the observations are background-like, and have confidence levels in the signals of 19% at best, we conclude that the excess of 2000a is not confirmed by the remaining data.

Table 12: Numerical study of the excess observed in period 2000a. In this data set, 10 events are observed while 3.7±0.6 are expected (Table 7). The entire excess is attributed to a signal, and predictions are made for the complementary data sets, for three mass hypotheses of an example hA signal. For every hypothesis, the observation and expected background correspond to the complementary data taken above threshold (see Table 7), and the corresponding confidence levels in the background and signal hypotheses are given.

Mass (GeV/c^2)	Rate (2000a)	Rate (compl.)	Bkg.	Data	CL_b	CL_s
(m_h,m_A)=(90,90)	6.3	~ 10	10.0	10	46%	10%
(95,95)	6.3	~ 5	6.8	8	63%	19%
(100,100)	6.3	~ 3	2.0	2	41%	8%

As a further illustration, the expected and observed mass distributions are shown in Figure 13, for the 2000a data set, and the complementary 1999 and 2000b sets. Shown is the distribution obtained when choosing the jet pairing so that the dijet mass difference is minimized; an example signal with (m_h,m_A)=(95,95) GeV/c^2 is superimposed, normalized as above (a lower mass signal is strongly disfavoured according to the results of Table 12). The mass distribution when all pairings enter (i.e., each event contributes three times) is also shown.

The upper limit on $C^2_{hA\to 4b}$ as a function of m_h+m_A is shown in Figure 14 for equal h and A masses as well as for large mass differences. In these figures, the observed result is compared to the expected limits, allowing a comparison of the data with the SM background predictions. The agreement is well within 2 standard deviations over the whole range of mass hypotheses in the case of equal h and A masses: there, the results are given by the LEP1 analysis of Section 2.1 up to about 90 GeV/c^2 in m_h+m_A, with limits on $C^2_{hA\to 4b}$ between $\sim$ 0.1% and 10%, and by the LEP2 MSSM analysis of [5] at higher masses, with limits on $C^2_{hA\to 4b}$ around 10% up to 160 GeV/c^2. For full strength production and decay, a mass limit on m_h and m_A of 90.9 GeV/c^2 is reached. In the case of large mass differences between the h and A bosons, the results are given by the LEP1 and the LEP2 analyses presented in this paper. As a result of the excess observed in the data of 2000a, there is a disagreement between the data and the SM background prediction in the upper limit on $C^2_{hA\to 4b}$. When m_A is fixed at 15 GeV/c^2(Figure 14) the disagreement amounts to 1.6 standard deviations for any m_h above $\sim$70 GeV/c^2. This also translates into a mass limit of 127.8 GeV/c^2on m_h+m_A, whereas 138.0 GeV/c^2 is expected on average from background experiments.

Numerical values for the observed exclusions are given in Table 24.

4.2.2 The four-τ search

The results of the hA$\to 4\tau$ analysis are shown in the (m_h,m_A) plane in Figure 12 and as a function of m_h+m_A for mass-degenerate h and A bosons in Figure 15. In the case of no suppression, this very sensitive search allows a large range of masses to be excluded, from the $\tau^+\tau^-$ threshold up to around 10 GeV/c^2 below the kinematical limit. For equal h and A masses, this translates into a mass limit of 93.6 GeV/c^2. Limits on $C^2_{hA\to 4\tau}$ are very strong, e.g. below 10% up to 140 GeV/c^2 in m_h+m_A for equal masses, allowing large portions of the mass plane to be excluded even up to $C^2_{hA\to 4\tau}$ $\sim$0.25, as shown in

Figure 12. Finally, Figure 15 also shows the results when one Higgs boson mass is fixed at 4 GeV/c^2. In this case, full strength production is excluded up to m_h,m_A= 158.1 GeV/c^2.

Numerical values for the observed exclusions are given in Table 25.

4.2.3 hZ with h→$b\bar{b}$ and h→$\tau^+\tau^-$

The upper limits on the suppression factors for hZ production followed by a direct decay of the h boson into τ lepton or b quark pairs, are shown as a function of m_h in Figure 16. For full strength production and decay, mass limits of 112.4 and 114.6 GeV/c^2 on m_h are obtained in the two channels, respectively (the mass limit in the $\tau^+\tau^-$ channel is not absolute, since there is an unexcluded region around m_h= 40 GeV/c^2). Upper limits on the suppression factors lower than 10% are obtained for m_h from the $b\bar{b}$ threshold up to 85 GeV/c^2 in the case of b decays. The limits are much weaker in the case of τ decays with upper bounds of 20% for m_h between 50 and 90 GeV/c^2.

Numerical values for the observed exclusions are given in Tables 26 and 27.

4.3 hA and hZ production: cascade decays

The analysis described in Section 3.1 is applied to the search for Higgs bosons involving cascade decays. Compared to the previous section, the only differences are the signal selection efficiencies, which are sensitive to the details of the final state. The primary hA and hZ production rates are the same as above.

Results on the final state with six b quarks, originating from hA production with intermediary decay of the h boson into two A bosons, are displayed in Figure 12. The high number of b quarks in the final state makes the search sensitive even for small suppression factors. For full strength production and decay, the limit on m_h is 114.5 GeV/c^2 when $m_A \sim m_h/2$, and 136.3 GeV/c^2 when m_A= 12 GeV/c^2.

Production of four b quarks in addition to a Z boson through the process hZ→(AA)Z, is constrained as shown in Figure 12. The m_h range covered is bounded from above because of the high mass of the associated Z boson. In the case of no suppression (in other words, if this channel is dominant), the present analysis constrains the h mass to be above ∼95 GeV/c^2, for any m_A between the b quark decay threshold and $m_h/2$.

The similar hA→h(hZ) process is found to be unconstrained by the present work. The reasons are that the hA cross-section decreases much faster than the hZ cross-section when approaching the kinematic limit, leading to reduced sensitivity. Furthermore, the excess observed in the data taken in 2000a (see Table 7 and the discussion given in the previous section) is enough to forbid any exclusion in this channel. This conclusion also applies to the (AZ)A process, as argued in Section 1.1.

Numerical values for the observed exclusions are given in Tables 28 and 29.

5 Conclusions

Searches for Higgs production have been performed in various channels, using the data recorded by DELPHI at LEP2, relying extensively on a multi-purpose b-tagging analysis. The much studied hA→4b channel has been revisited and extended sensitivity towards large h and A mass differences was obtained. The decay h→AA was also considered and searched for in hA and hZ production. In these three cases large portions of the (m_h,m_A) plane are excluded, depending on a global suppression factor. The decay A→hZ was also studied but was found unconstrained.

Four-b final states were searched for in the LEP1 data, in the hA channel and in the Yukawa process. The results of the hA channel contribute to the coverage of the (m_h,m_A) plane at low masses. The search for the Yukawa process allowed the enhancement of the h and A coupling to b quarks to be constrained for a large mass range of these bosons. The $b\bar{b}\tau^+\tau^-$ final state was investigated in the context of the Yukawa process, and is constrained over the same mass range.

Finally, models in which different Higgs doublets couple preferentially to quarks or to leptons will predict dominant heavy-lepton decays. The four-τ final state from Yukawa production was searched for at LEP1. The hA$\rightarrow 4\tau$ channel was investigated at LEP2, and strongly constrained by the present analysis.

The emphasis of this work is on the model-independence of the results. All results are presented in a form that allows their reinterpretation in a large class of models of the electroweak scalar sector.

Acknowledgements

We are greatly indebted to our technical collaborators, to the members of the CERN-SL Division for the excellent performance of the LEP collider, and to the funding agencies for their support in building and operating the DELPHI detector.
We acknowledge in particular the support of
Austrian Federal Ministry of Education, Science and Culture, GZ 616.364/2-III/2a/98,
FNRS–FWO, Flanders Institute to encourage scientific and technological research in the industry (IWT), Belgium,
FINEP, CNPq, CAPES, FUJB and FAPERJ, Brazil,
Czech Ministry of Industry and Trade, GA CR 202/99/1362,
Commission of the European Communities (DG XII),
Direction des Sciences de la Matière, CEA, France,
Bundesministerium für Bildung, Wissenschaft, Forschung und Technologie, Germany,
General Secretariat for Research and Technology, Greece,
National Science Foundation (NWO) and Foundation for Research on Matter (FOM), The Netherlands,
Norwegian Research Council,
State Committee for Scientific Research, Poland, SPUB-M/CERN/PO3/DZ296/2000, SPUB-M/CERN/PO3/DZ297/2000, 2P03B 104 19 and 2P03B 69 23(2002-2004)
FCT - Fundação para a Ciência e Tecnologia, Portugal,
Vedecka grantova agentura MS SR, Slovakia, Nr. 95/5195/134,
Ministry of Science and Technology of the Republic of Slovenia,
CICYT, Spain, AEN99-0950 and AEN99-0761,
The Swedish Natural Science Research Council,
Particle Physics and Astronomy Research Council, UK,
Department of Energy, USA, DE-FG02-01ER41155.
EEC RTN contract HPRN-CT-00292-2002.

References

[1] The LEP Collaborations ALEPH, DELPHI, L3, OPAL, the LEP Electroweak Working Group, the SLD Electroweak and Heavy Flavour Groups, CERN-EP/2003-091;

The LEP Collaborations ALEPH, DELPHI, L3, OPAL, the LEP Higgs Working Group, Phys. Lett. **B565** (2003) 61.
[2] S. Glashow and S. Weinberg, Phys. Rev **D15** (1977) 1958.
[3] DELPHI Collaboration, CERN-EP/2003-087.
[4] DELPHI Collaboration, DELPHI 2003-005 CONF 628, submitted to the 2003 winter conferences.
[5] DELPHI Collaboration, Eur. Phys. J. **C32** (2004) 145, and references therein.
[6] ALEPH Collaboration, Phys. Lett. **B526** (2002) 191;
ALEPH Collaboration, Phys. Lett. **B544** (2002) 16;
ALEPH Collaboration, Phys. Lett. **B544** (2002) 25;
L3 Collaboration, Phys. Lett. **B534** (2002) 28;
L3 Collaboration, Phys. Lett. **B545** (2002) 30;
L3 Collaboration, Phys. Lett. **B583** (2004) 14;
OPAL Collaboration, Eur. Phys. J. **C18** (2001) 425;
OPAL Collaboration, Eur. Phys. J. **C23** (2002) 397;
OPAL Collaboration, Eur. Phys. J. **C27** (2003) 483.
[7] J. F. Gunion, H. E. Haber, G. Kane, S. Dawson, *The Higgs Hunter's Guide*, Addison-Wesley Publishing Company.
[8] E. Gross, G. Wolf and B. Kniehl, Z. Phys. **C63** (1994) 417.
[9] P. Janot, in CERN Report 96-01, Vol. 2 (1996) 309.
[10] J. Kalinowski, M. Krawczyk, Phys. Lett. **B361** (1995) 66;
J. Kalinowski, M. Krawczyk, Warsaw preprint IFT-96-03.
[11] M. Carena, J. R. Ellis, A. Pilaftsis, C.E.M. Wagner, Nucl. Phys. **B586** (2000) 92.
[12] DELPHI Collaboration, Nucl. Instr. Meth **A303** (1991) 233;
DELPHI Silicon Tracker Group, Nucl. Instr. Meth **A412** (1998) 304.
[13] T. Sjöstrand, Comp. Phys. Comm. **39** (1986) 347. Version 6.156 is used.
[14] S. Jadach, B.F.L. Ward, and Z. Was, Comp. Phys. Comm. **130** (2000) 260;
S. Jadach, B.F.L. Ward, and Z. Was, Phys. Rev. **D63** (2001) 113009.
[15] F.A. Berends, R. Pittau, R. Kleiss, Comp. Phys. Comm. **85** (1995) 437.
[16] E. Accomando and A. Ballestrero, Comp. Phys. Comm. **99** (1997) 270;
E. Accomando, A. Ballestrero and E. Maina, Comp. Phys. Comm. **150** (2003) 166.
[17] DELPHI Collaboration, Nucl. Inst. Meth. **A378** (1996) 57.
[18] DELPHI Collaboration, Phys. Lett. **B479** (2000) 89.
[19] DELPHI Collaboration, Eur. Phys. J. **C32** (2004) 185, and references therein.
[20] A.L. Read, in CERN Report 2000-005 (2000) 81.
[21] D. J. Miller, M. H. Seymour, Phys. Lett. **B435** (1998) 213.
[22] ALEPH Collaboration, Phys. Lett. **B434** (1998) 437;
DELPHI Collaboration, Phys. Lett. **B462** (1999) 425;
OPAL Collaboration, Eur. Phys. J. **C18** (2001) 447;
SLD Collaboration, Phys. Lett. **B507** (2001) 61.
The above measurements were averaged assuming uncorrelated systematics.
[23] S. Catani et al., Phys. Lett. **B269** (1991) 432;
N. Brown, W. J. Stirling, Z. Phys. **C53** (1992) 629.
[24] DELPHI Collaboration, Phys. Lett. **B552** (2003) 127.
[25] DELPHI Collaboration, DELPHI 99-76 CONF 263, submitted to the 1999 summer conferences.

Figure 1: Higgs boson production processes at LEP.

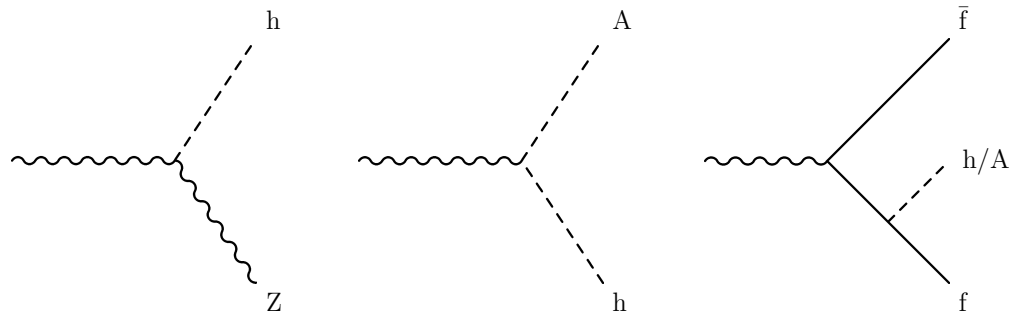

Bjorken process Pair production Yukawa process

Figure 2: Non-fermionic Higgs boson decay modes.

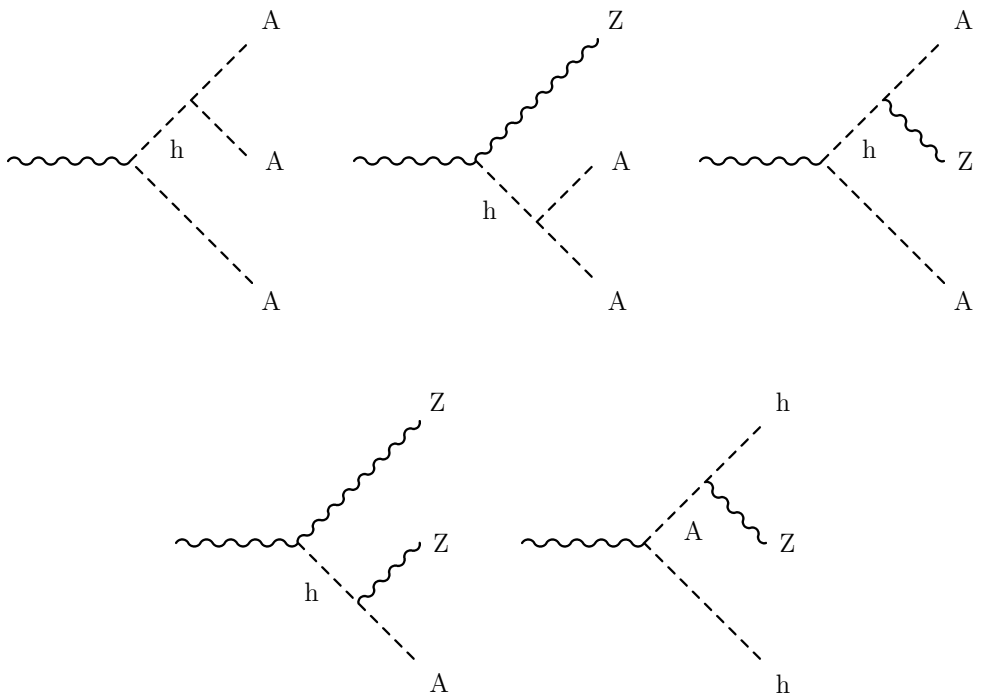

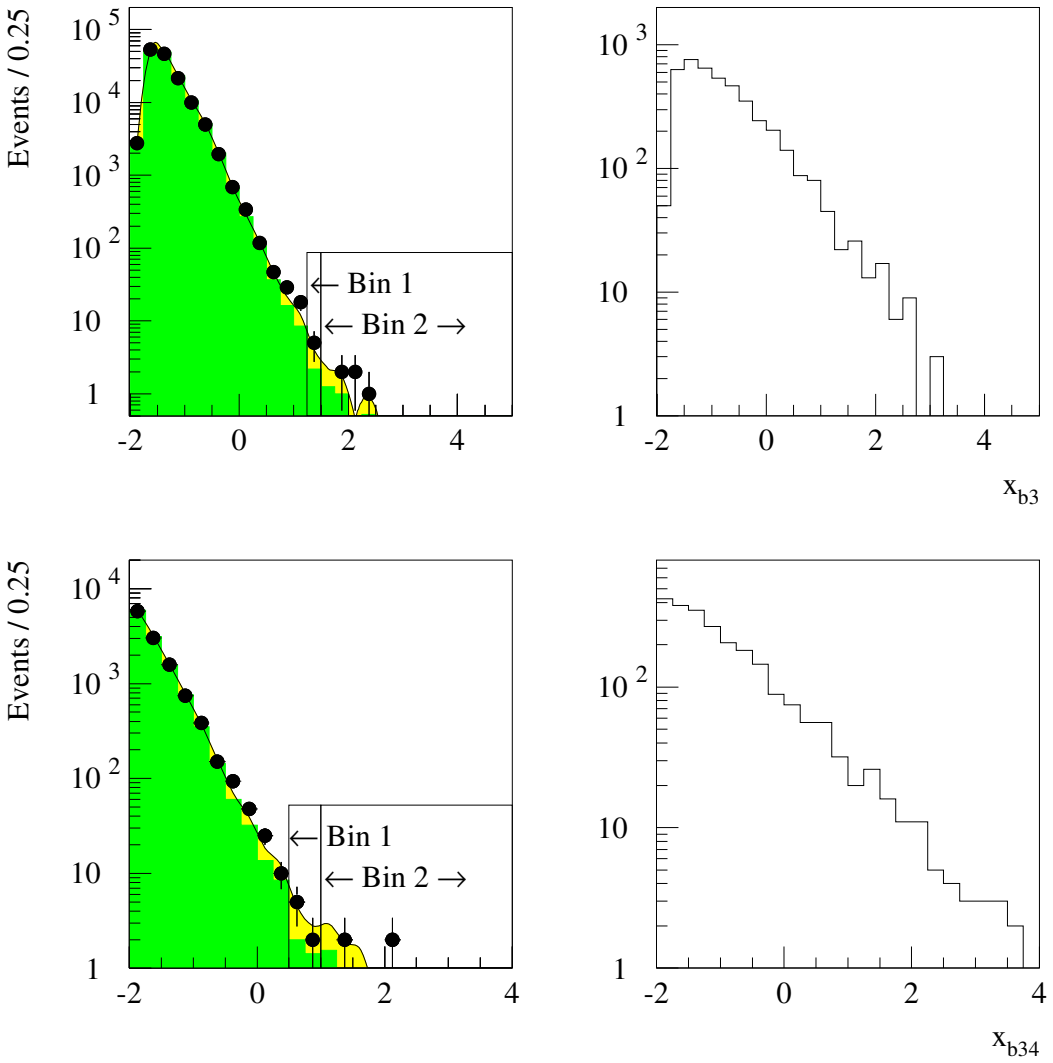

Figure 3: Comparison between data and simulation for the distributions of the final b-tagging variables of the Yukawa four-b analyses, as defined in the text (left). The points are the data. On top of the dark histogram, representing the Standard Model $q\bar{q}$ background with $g_{bb} = 1.5\,10^{-3}$, a fit to the data suggests a larger gluon splitting value (see text). Distributions expected for a $b\bar{b}(h \to b\bar{b})$ signal are shown on the right, with arbitrary normalization.

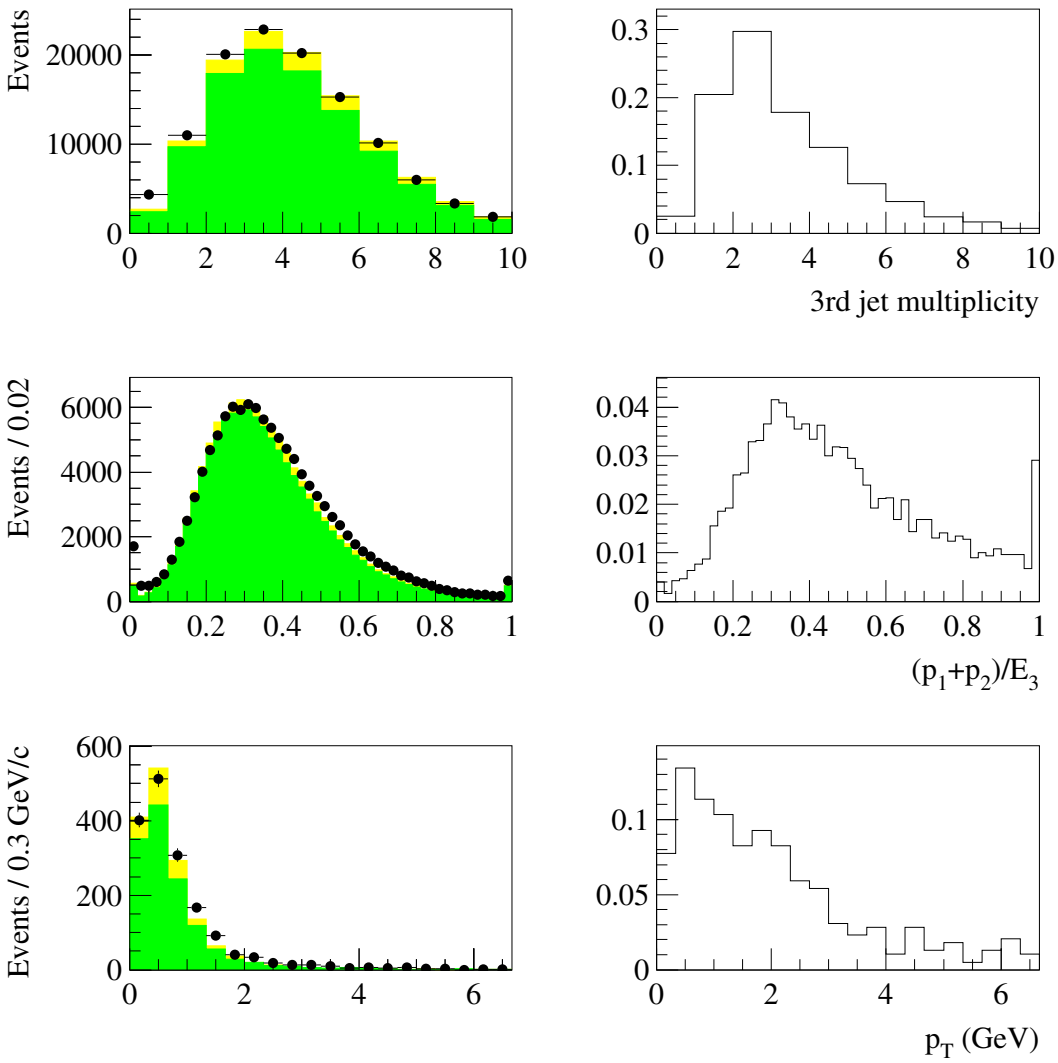

Figure 4: Comparison between data and simulation for the distributions of some variables used in the $b\bar{b}\tau^+\tau^-$ analysis, at the preselection level. On the left, the points are the data, the dark histograms represent the Standard Model $q\bar{q}$ background, and the light histograms represent the $q\bar{q}l^+l^-$ (l=e, μ, τ) contribution. The histograms on the right show distributions for a $b\bar{b}(h\rightarrow\tau^+\tau^-)$ signal, with arbitrary normalization.

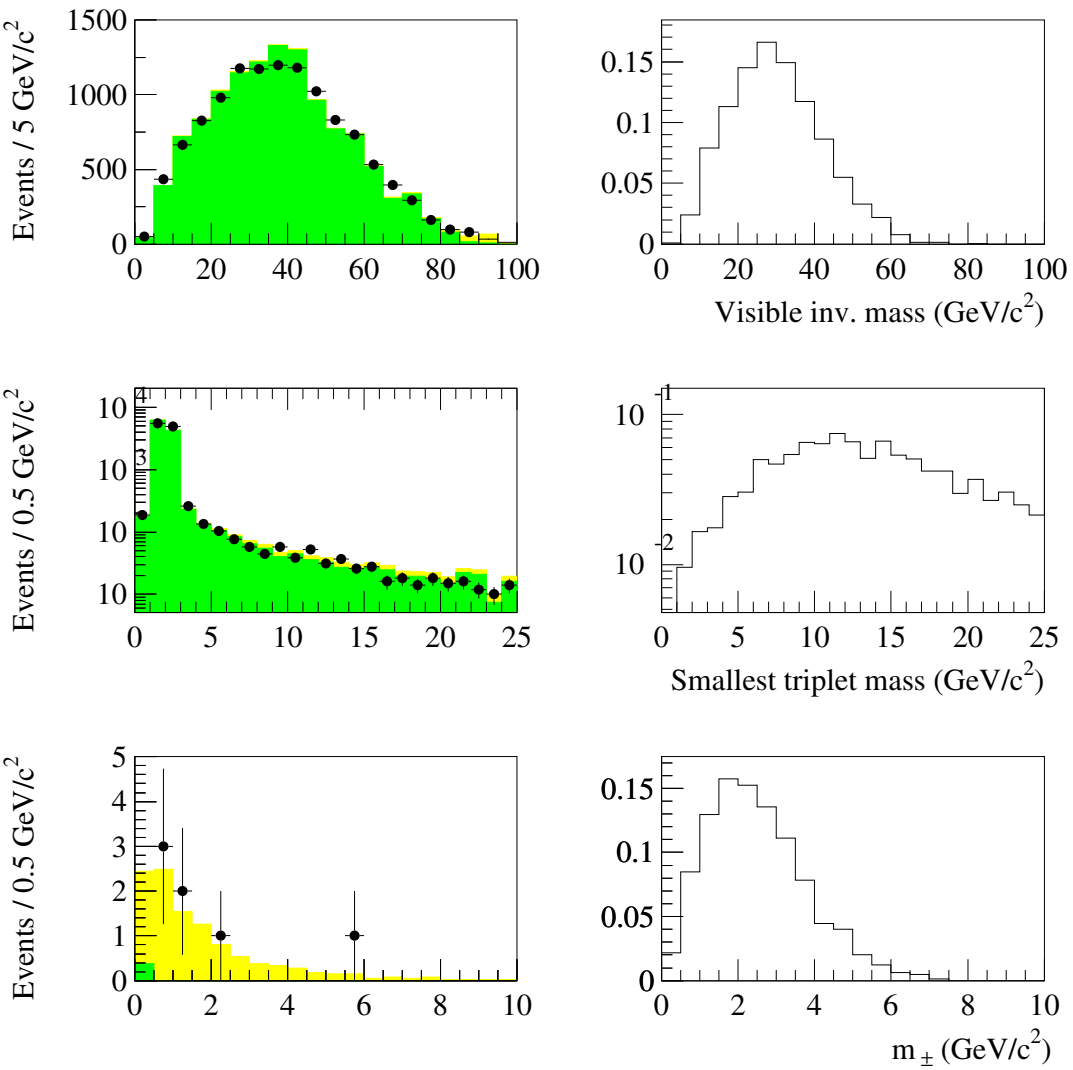

Figure 5: Comparison between data and simulation for the distributions of some variables used in the four-τ four-prong analysis. The visible mass and the lowest triplet mass are shown at the preselection level. The $m_\pm$ mass is shown just before the final selection cut. On the left, the points are the data, the dark histograms represent the Standard Model $q\bar{q}$ and $\tau^+\tau^-$ backgrounds, and the light histograms represent the various four-fermion contributions. The histograms on the right show distributions for a $\tau^+\tau^-(h \rightarrow \tau^+\tau^-)$ signal, with arbitrary normalization.

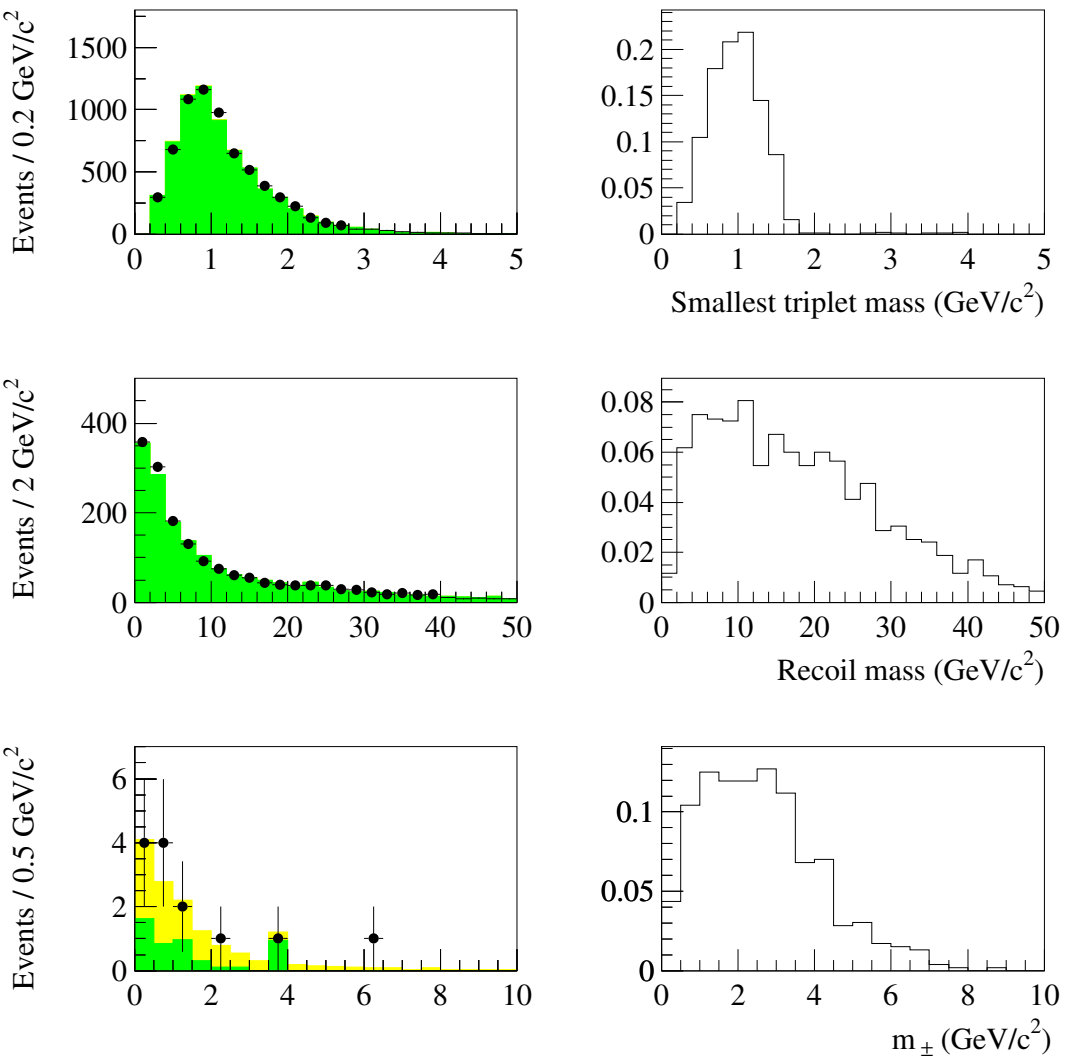

Figure 6: Comparison between data and simulation for the distributions of some variables used in the four-τ six-prong analysis. The lowest triplet mass and the mass of the system recoiling against it are shown at the preselection level. The $m_\pm$ mass is shown just before the final selection cut. On the left, the points are the data, the dark histograms represent the Standard Model $q\bar{q}$ and $\tau^+\tau^-$ backgrounds, and the light histograms represent the four-fermion contributions. The histograms on the right show distributions for a $\tau^+\tau^-(h\rightarrow\tau^+\tau^-)$ signal, with arbitrary normalization.

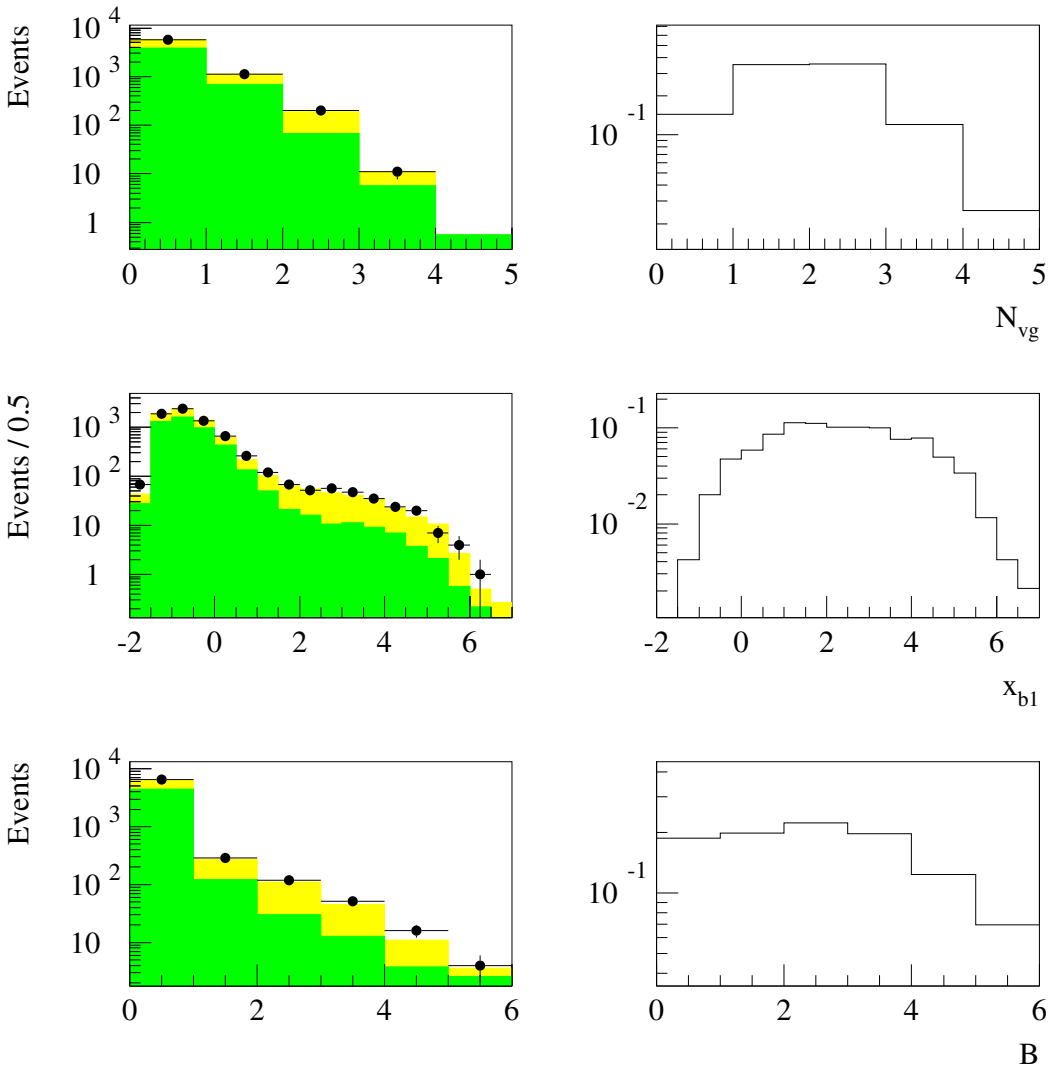

Figure 7: Comparison between data and simulation for the distributions of some variables used in the LEP2 four-b search, at the preselection level. On the left, the points are the data, the dark histograms show the Standard Model four-fermion background, and the light histograms represent the two-fermion $q\bar{q}$ contribution. The histograms on the right show distributions for a (AA)Z$\rightarrow$ 4b+jets signal, with arbitrary normalization.

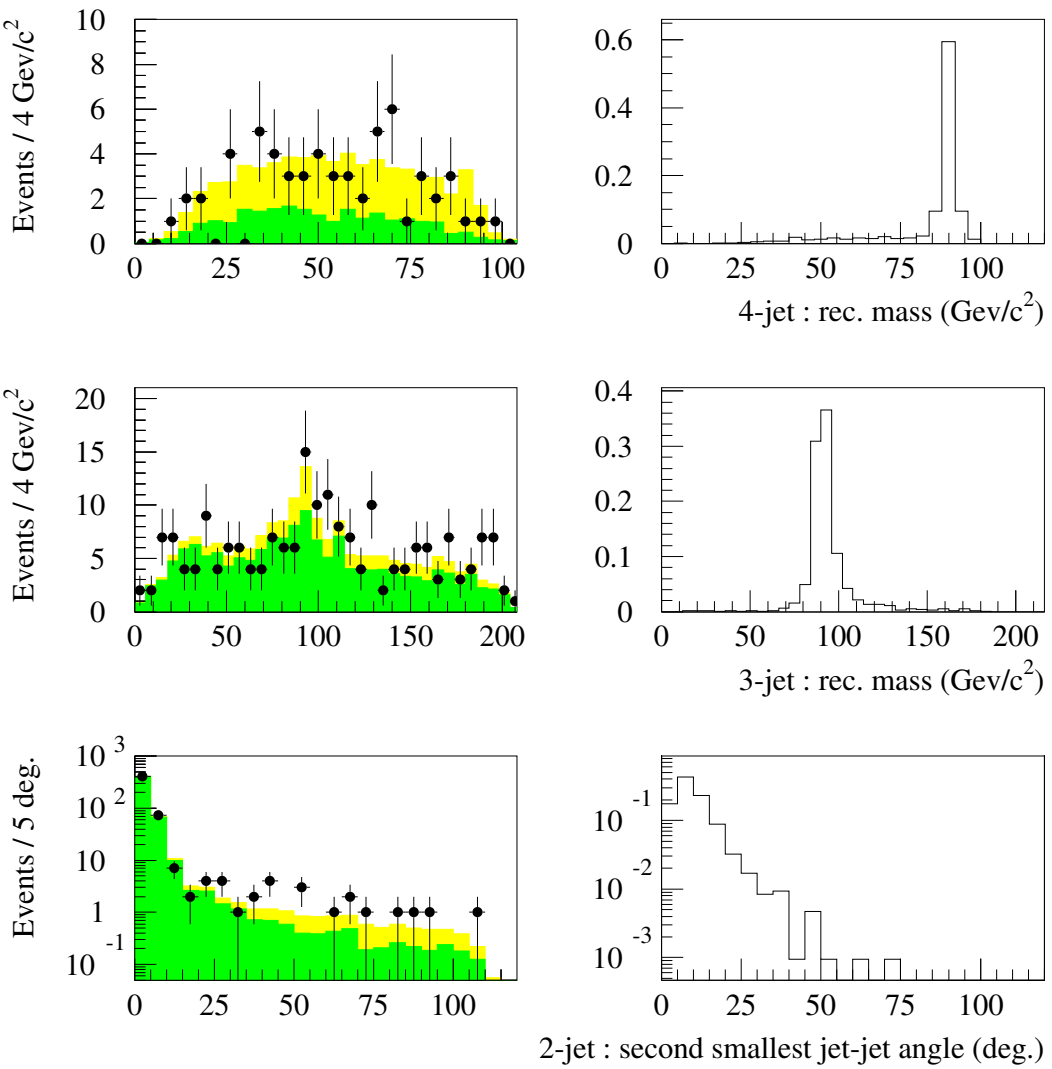

Figure 8: Comparison between data and simulation for the mass distributions used in the statistical interpretation of the four-τ analyses. On the left, the points are the data, the light histograms represent the four-lepton contributions, and the dark histograms represent the remaining two- and four-fermion processes. The four-jet and three-jet discriminants are shown at their respective preselection level; the two-jet discriminant is shown after the $\gamma\gamma$ rejection. The histograms on the right show distributions for three example signals: $(m_h,m_A) = (90,90)$, $(90,4)$, and $(4,4)$ GeV/c^2 for the four-jet, three-jet and two-jet analysis respectively. Normalization is arbitrary.

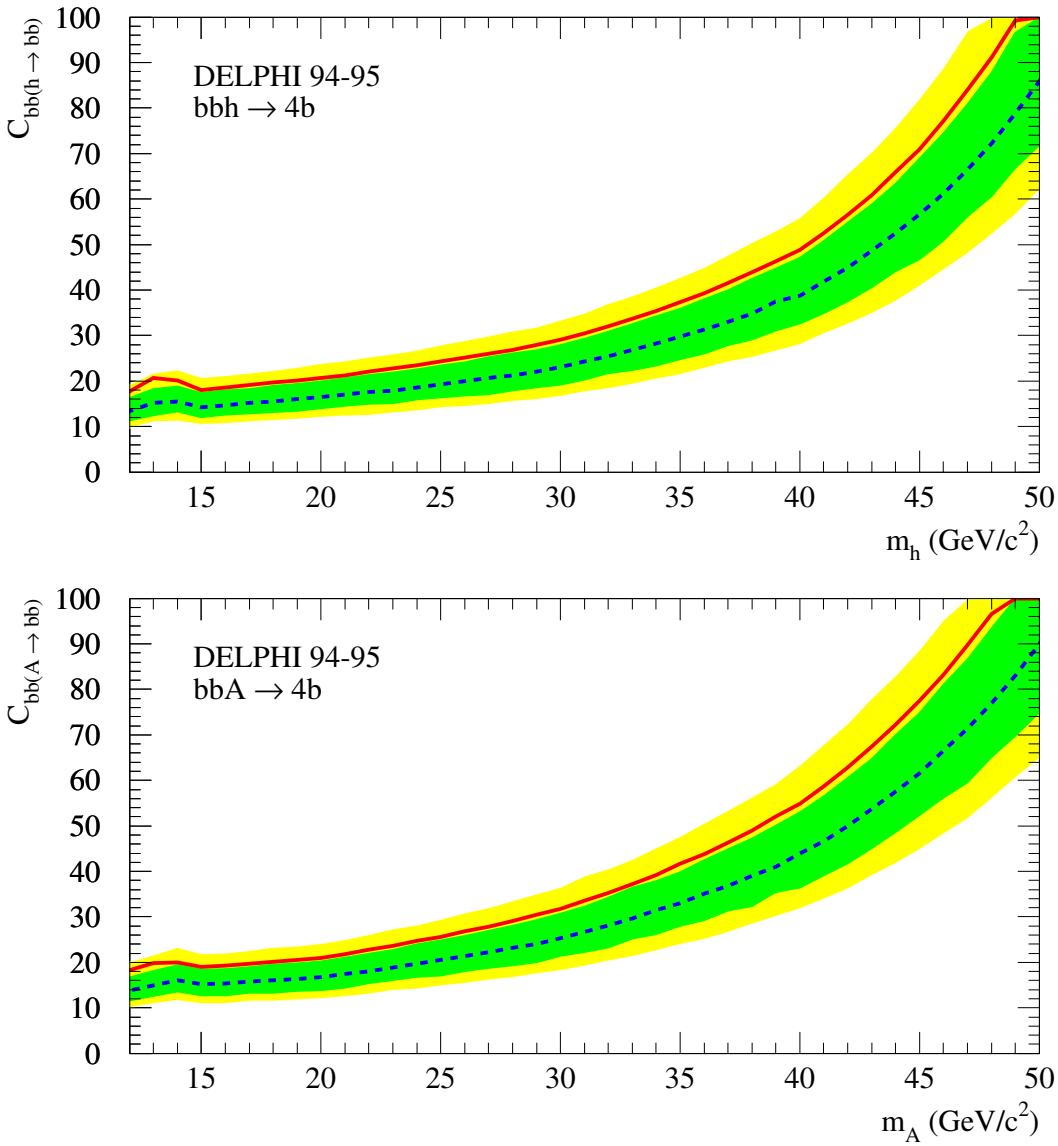

Figure 9: Upper limits on $C_{bb(h \to bb)}$ (top) and $C_{bb(A \to bb)}$ (bottom), defined in Section 1.1. The dashed line shows the average expectation for background experiments, and the full line shows the observation. The bands correspond to the 68.3% and 95.0% confidence intervals for background-only experiments. The excess observed in the data translates into an exclusion slightly weaker than expected. The discrepancy is about 1.2 standard deviations in the mass range $m_{h,A} > 15$ GeV, where the four-jet analysis is used. For lower masses the three-jet analysis is used, with a discrepancy just below 2 standard deviations.

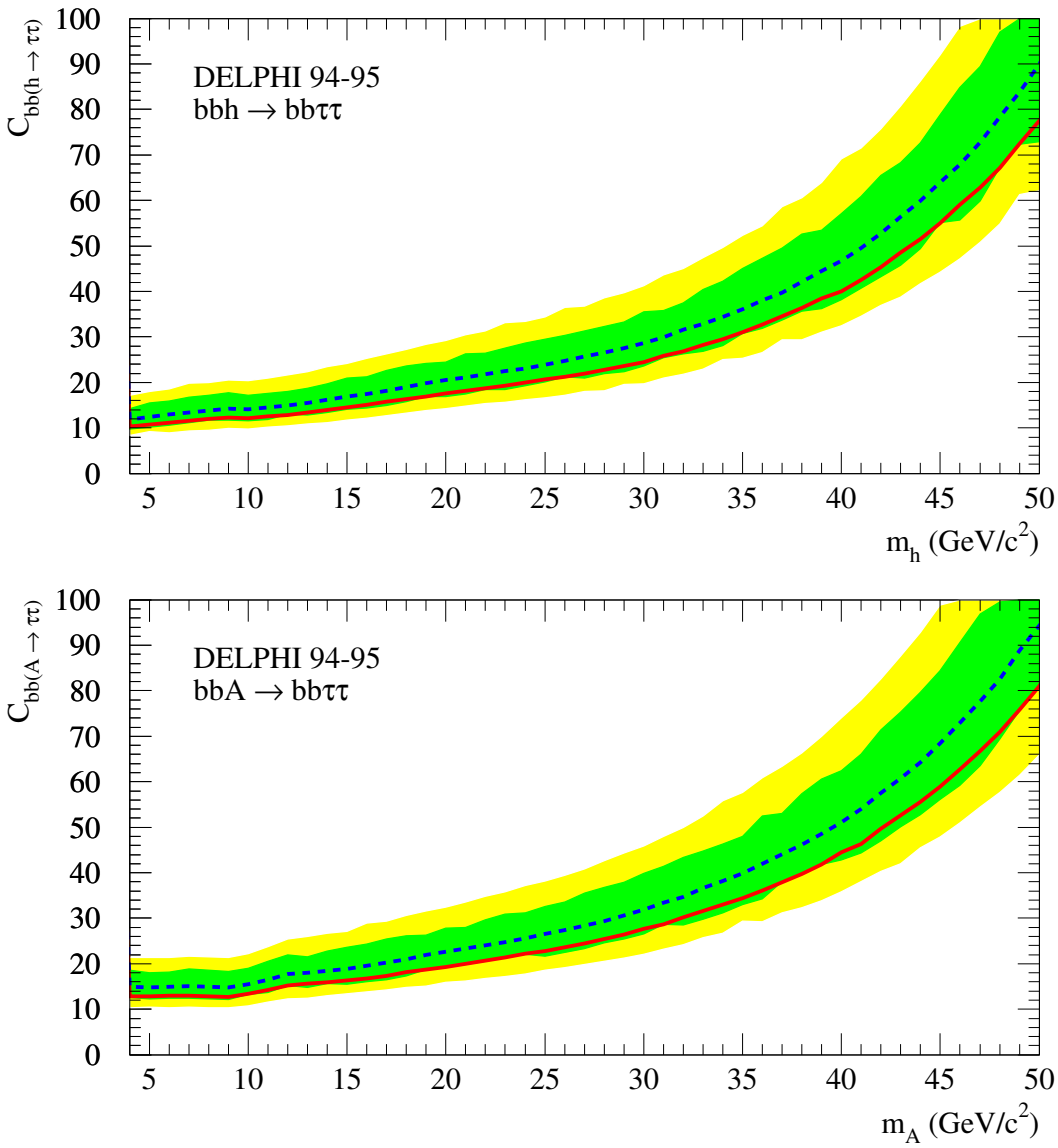

Figure 10: Upper limits on $C_{bb(h \to \tau\tau)}$ (top) and $C_{bb(A \to \tau\tau)}$ (bottom), defined in Section 1.1. The dashed line shows the average expectation for background experiments, and the full line shows the observation.The bands correspond to the 68.3% and 95.0% confidence intervals for background-only experiments.

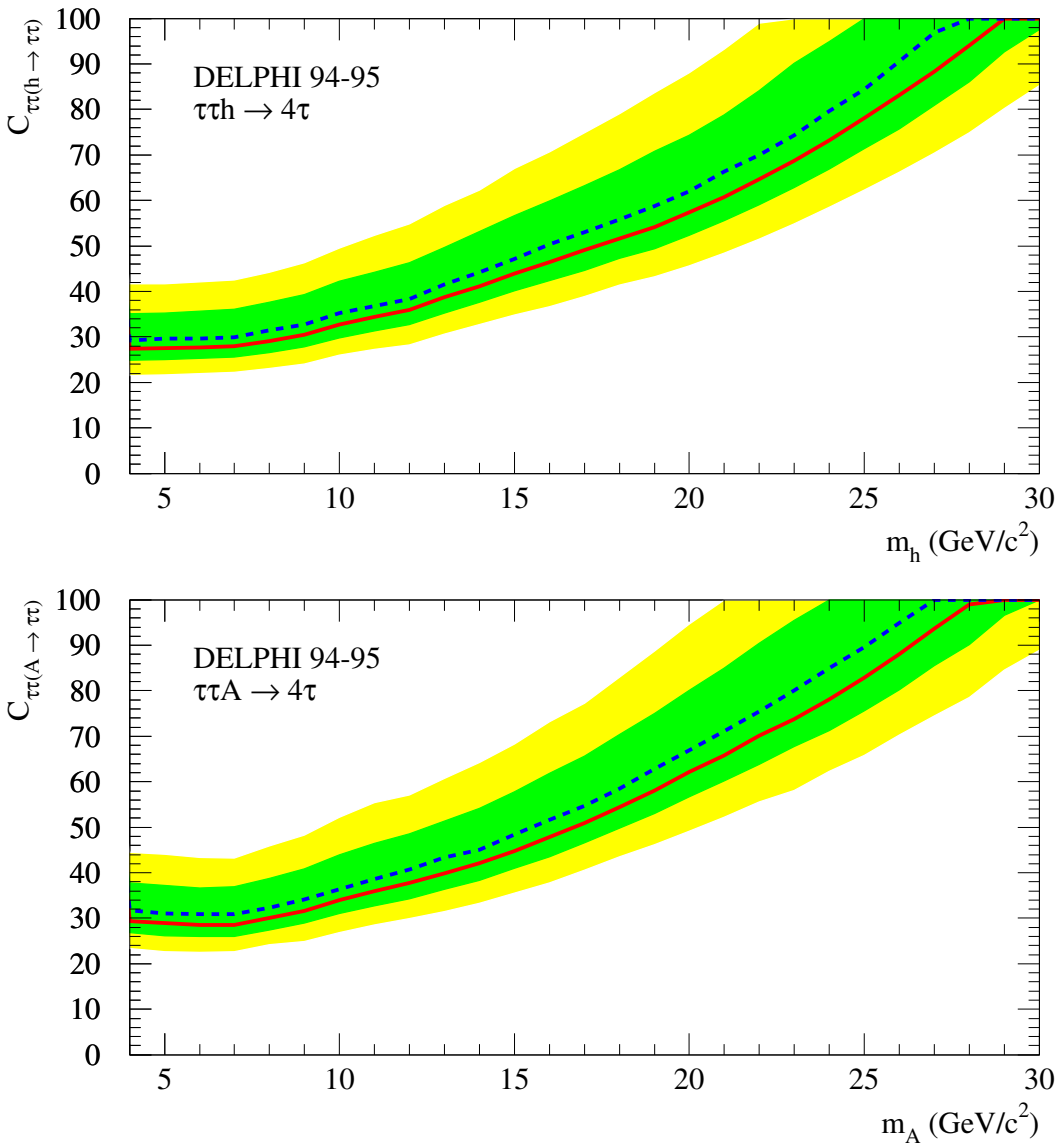

Figure 11: Upper limits on $C_{\tau\tau(h\to\tau\tau)}$ (top) and $C_{\tau\tau(A\to\tau\tau)}$ (bottom), defined in Section 1.1. The dashed line shows the average expectation for background experiments, and the full line shows the observation.The bands correspond to the 68.3% and 95.0% confidence intervals for background-only experiments.

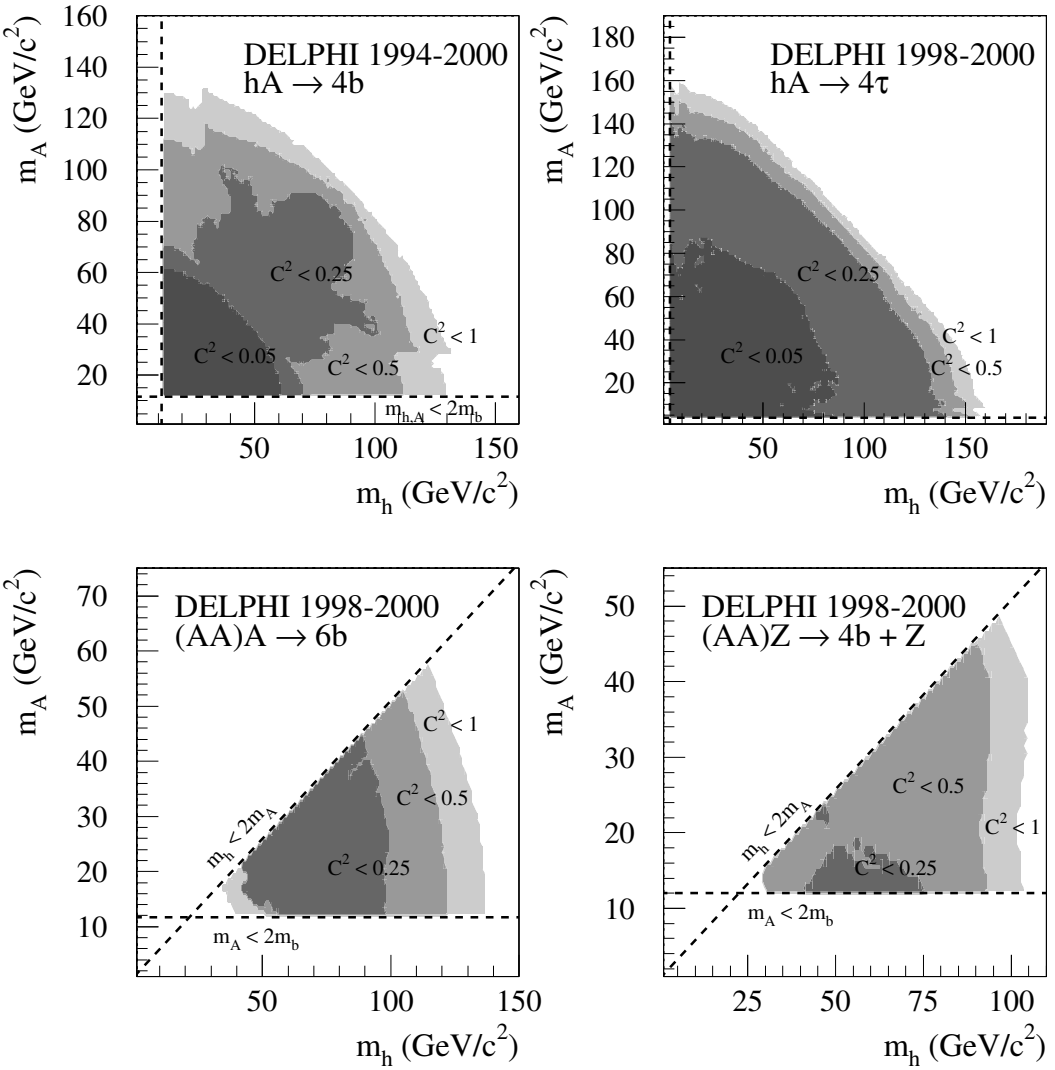

Figure 12: Excluded couplings in the (m_h,m_A) plane. Upper left: hA→4b ($C^2 \equiv C^2_{hA\to 4b}$); upper right: hA→4$\tau$ ($C^2 \equiv C^2_{hA\to 4\tau}$); lower left: (AA)A→6b ($C^2 \equiv C^2_{hA\to 6b}$); lower right: (AA)Z→4b+jets ($C^2 \equiv C^2_{Z(AA\to 4b)}$). The C^2 parameters are defined in Section 1.1. The three outer embedded regions correspond to excluded C^2 values of 1, 0.5, and 0.25 respectively; for the hA→4b final state (which includes LEP1 results) and the hA→4τ final state, the innermost region corresponds to excluded couplings smaller than 0.05.

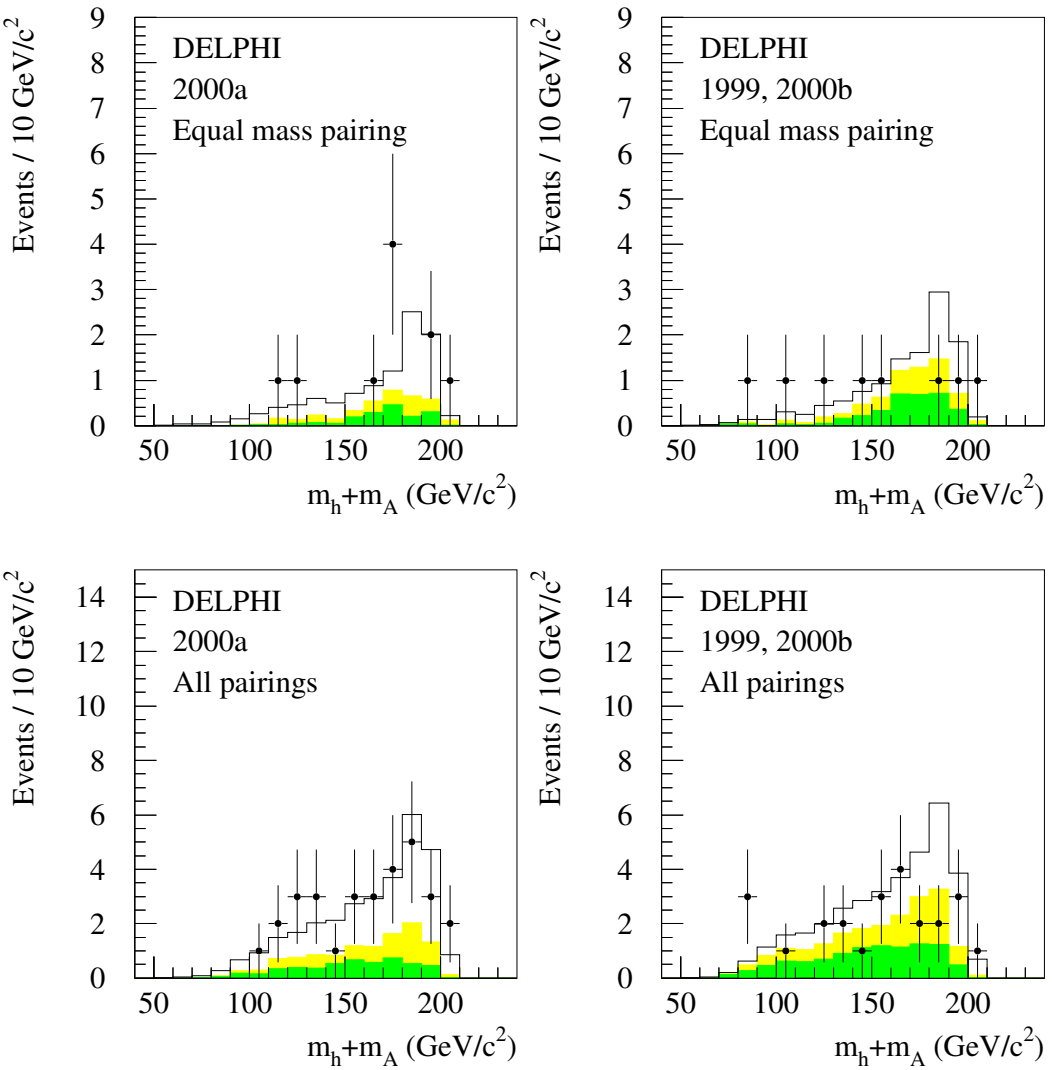

Figure 13: Distributions of m_h+m_A for the data taken in 2000a (left) and for the complementary data set (right). For both datasets, the mass distributions are given with the jet pairing chosen to minimize the dijet mass difference (above), and including all pairings (below). The points are the data; the light and dark histograms represent the Standard Model four-fermion and $q\bar{q}$ backgrounds, respectively. An hA signal (m_h=m_A= 95 GeV/c^2) is superimposed; it is normalized to the excess observed in 2000a, and to the corresponding expectation for the complementary dataset. The 1998 data are below the signal threshold and discarded.

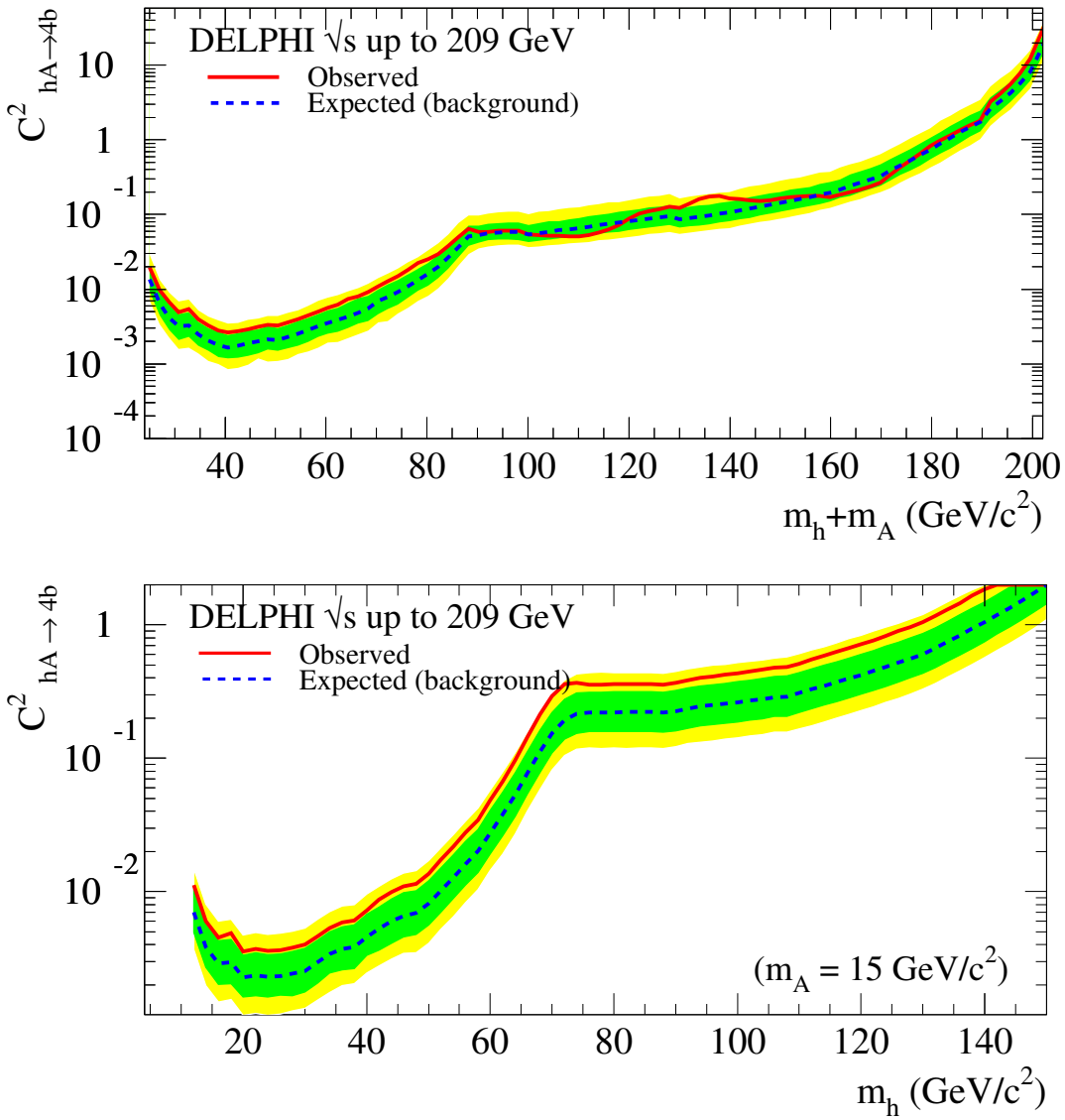

Figure 14: 95% CL upper bounds on the reduction factor $C^2_{hA\to 4b}$, as defined in Section 1.1. Results are presented for h and A bosons with equal masses (top) and with one mass fixed to 15 GeV/c^2 (bottom). The limits observed in the data (full curve) are shown together with the expected median limits in background process experiments (dashed curve). The bands correspond to the 68.3% and 95.0% confidence intervals for background-only experiments.

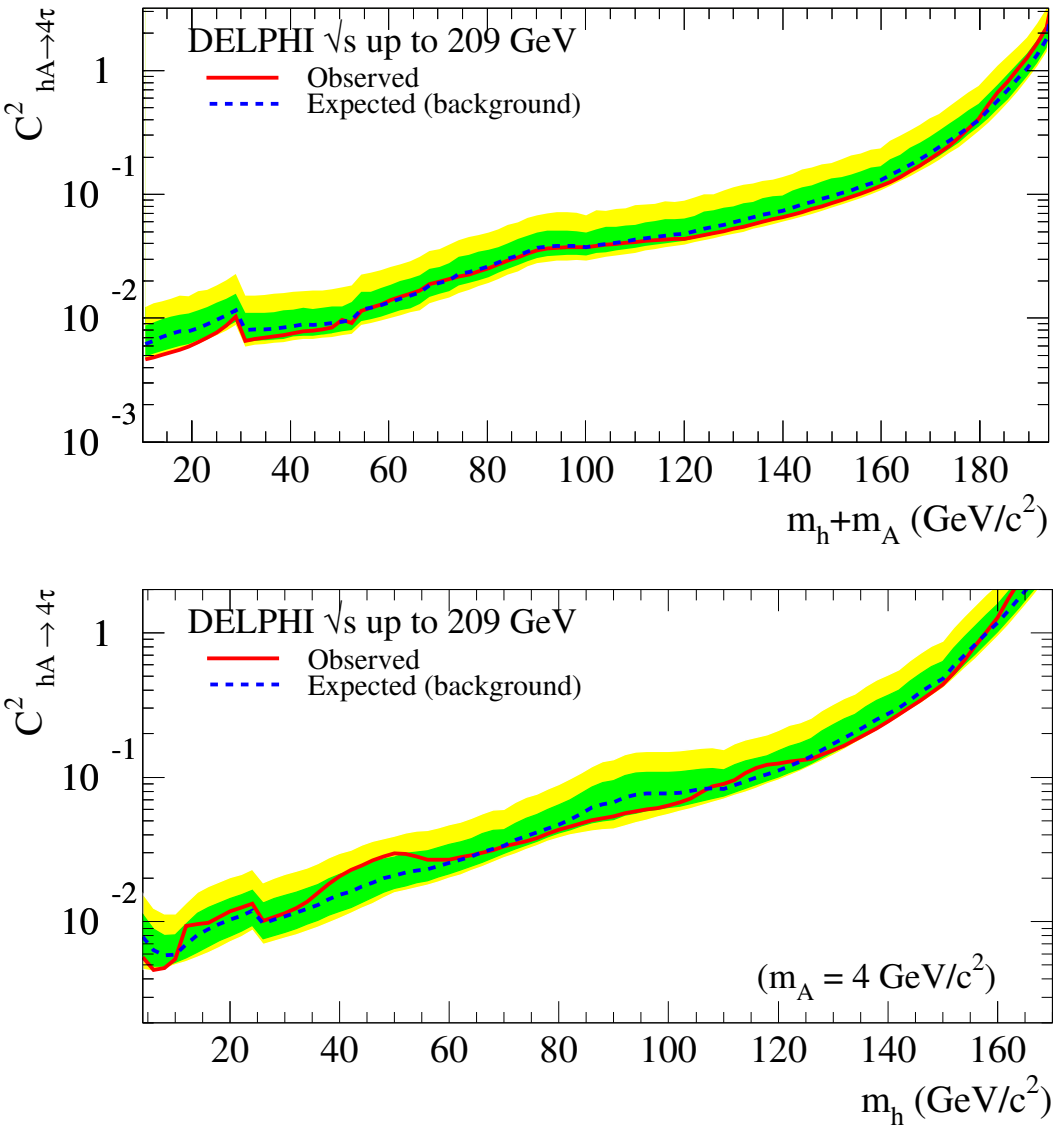

Figure 15: 95% CL upper bounds on the reduction factor $C^2_{hA\to4\tau}$, as defined in the text. Results are presented in the four-τ channel for h and A bosons with equal masses (top) and with one mass fixed to 4 GeV/c^2 (bottom). The limits observed in the data (full curve) are shown together with the expected median limits in background process experiments (dashed curve). The bands correspond to the 68.3% and 95.0% confidence intervals for background-only experiments.

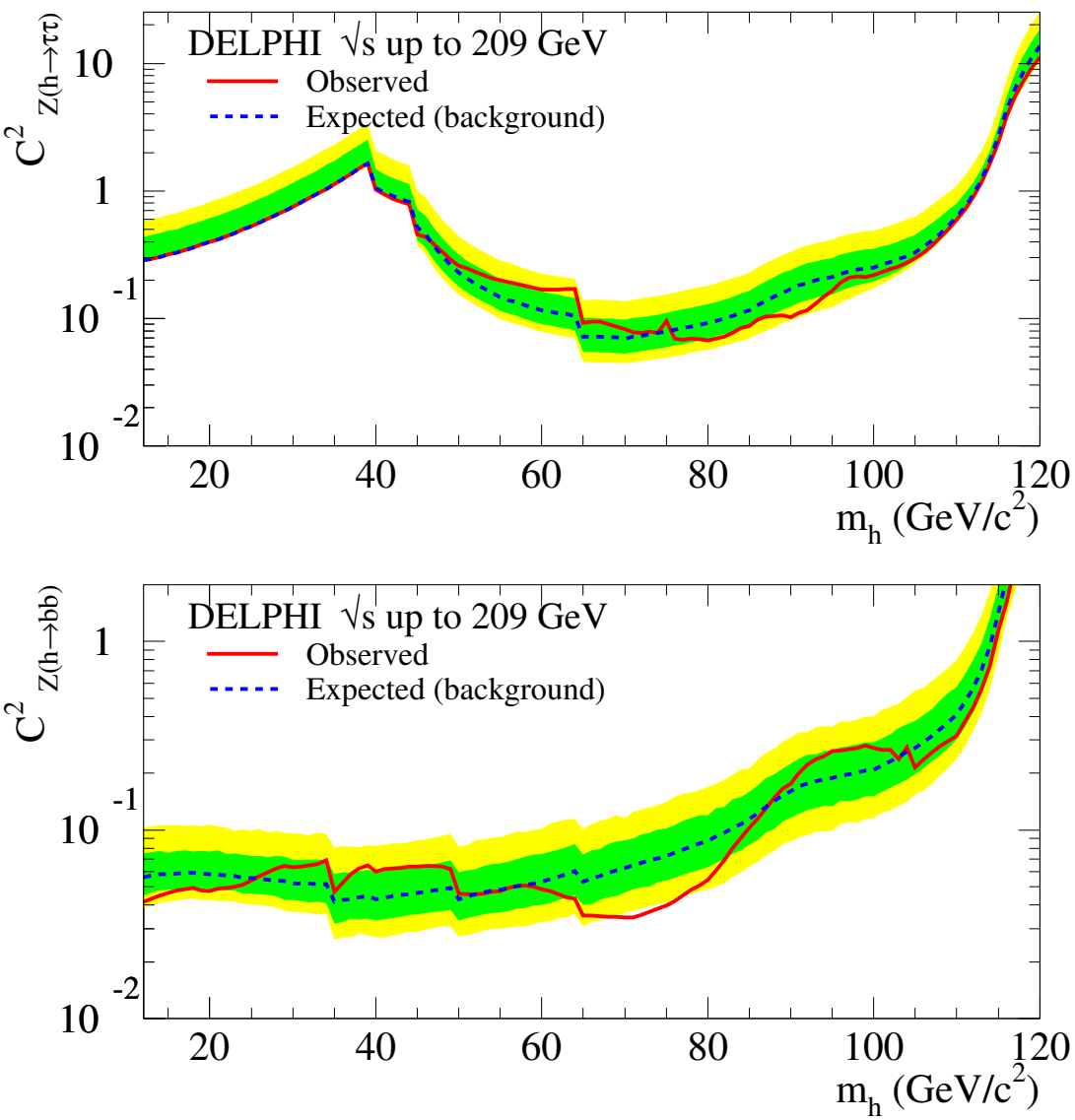

Figure 16: 95% CL upper bounds on the reduction factors $C^2_{Z(h\to\tau\tau)}$ and $C^2_{Z(h\to bb)}$, as defined in Section 1.1. The limits observed in the data (full curve) are shown together with the expected median limits in background process experiments (dashed curve). The bands correspond to the 68.3% and 95.0% confidence intervals for background-only experiments. The shape of the results in the τ channel is due to the sensitivity of the LEP2 analyses starting at 40 GeV/c^2 and to LEP1 analyses applied on subsets of the data sample only.

A Efficiencies

Signal efficiencies for all analyses presented in this paper are given below. The quoted uncertainties are statistical only.

Table 13: Signal efficiencies in the $b\bar{b}(h\to b\bar{b})$ and $b\bar{b}(A\to b\bar{b})$ channels (LEP1).

mass (GeV/c^2)	three-jet eff. (%)		four-jet eff. (%)	
	Bin 1	Bin 2	Bin 1	Bin 2
m_h= 11	0.5 ± 0.1	1.2 ± 0.2	0.4 ± 0.1	0.5 ± 0.1
13	0.6 ± 0.1	0.7 ± 0.1	0.7 ± 0.1	0.4 ± 0.1
15	0.4 ± 0.1	0.8 ± 0.1	0.9 ± 0.1	1.1 ± 0.1
20	0.5 ± 0.1	1.0 ± 0.1	1.1 ± 0.2	1.5 ± 0.2
30	0.7 ± 0.1	1.2 ± 0.2	1.8 ± 0.2	2.1 ± 0.2
40	0.6 ± 0.1	1.5 ± 0.2	1.8 ± 0.2	2.4 ± 0.2
50	0.6 ± 0.1	0.9 ± 0.1	1.3 ± 0.2	1.8 ± 0.2
m_A= 11	0.6 ± 0.1	1.4 ± 0.2	0.9 ± 0.1	0.5 ± 0.1
13	0.5 ± 0.1	1.3 ± 0.2	0.8 ± 0.1	0.7 ± 0.1
15	0.5 ± 0.1	1.0 ± 0.1	1.1 ± 0.2	1.3 ± 0.2
20	0.5 ± 0.1	1.1 ± 0.2	1.4 ± 0.2	1.8 ± 0.2
30	0.5 ± 0.1	1.3 ± 0.2	1.7 ± 0.2	2.2 ± 0.2
40	0.4 ± 0.1	1.5 ± 0.2	1.8 ± 0.2	2.2 ± 0.2
50	0.5 ± 0.1	1.1 ± 0.1	1.7 ± 0.2	1.8 ± 0.2

Table 14: Signal efficiencies in the hA→4b channel (LEP1). The efficiencies are symmetric in m_h and m_A.

mass (GeV/c^2)	three-jet eff. (%)		four-jet eff. (%)	
m_A,m_h	Bin 1	Bin 2	Bin 1	Bin 2
12,20	0.8 ± 0.1	1.7 ± 0.2	1.2 ± 0.1	1.1 ± 0.1
12,30	0.9 ± 0.1	2.0 ± 0.2	1.5 ± 0.1	1.4 ± 0.1
12,40	1.0 ± 0.1	1.8 ± 0.2	1.3 ± 0.1	1.1 ± 0.1
12,50	1.0 ± 0.1	1.9 ± 0.2	1.3 ± 0.1	1.2 ± 0.1
12,60	0.8 ± 0.1	1.5 ± 0.1	0.9 ± 0.1	0.8 ± 0.1
12,70	0.4 ± 0.1	0.7 ± 0.1	0.4 ± 0.1	0.3 ± 0.1
20,20	0.9 ± 0.1	2.0 ± 0.2	2.4 ± 0.2	3.4 ± 0.2
20,30	0.9 ± 0.1	1.6 ± 0.2	2.4 ± 0.2	3.5 ± 0.3
20,40	0.7 ± 0.1	1.3 ± 0.1	1.8 ± 0.2	2.5 ± 0.2
20,50	0.7 ± 0.1	1.3 ± 0.2	1.6 ± 0.2	2.0 ± 0.2
20,60	0.7 ± 0.1	1.1 ± 0.1	1.3 ± 0.1	1.2 ± 0.1
30,30	0.7 ± 0.1	1.8 ± 0.2	2.0 ± 0.2	2.7 ± 0.2
30,40	0.6 ± 0.1	1.2 ± 0.1	1.6 ± 0.2	2.4 ± 0.2
30,50	0.4 ± 0.1	1.3 ± 0.1	1.7 ± 0.2	2.1 ± 0.2
40,40	0.6 ± 0.1	1.1 ± 0.1	1.8 ± 0.2	2.0 ± 0.2

Table 15: Signal efficiencies in the $b\bar{b}(h\to\tau^+\tau^-)$ and $b\bar{b}(A\to\tau^+\tau^-)$ channels (LEP1).

mass (GeV/c^2)	efficiency (%)	mass (GeV/c^2)	efficiency (%)
m_h= 4	0.8 ± 0.1	m_A= 4	1.0 ± 0.1
7	1.1 ± 0.1	7	1.4 ± 0.1
9	1.3 ± 0.1	9	1.8 ± 0.1
10	1.5 ± 0.1	10	1.8 ± 0.1
12	1.7 ± 0.1	12	1.7 ± 0.1
15	1.9 ± 0.1	15	2.0 ± 0.1
20	2.2 ± 0.2	20	2.3 ± 0.2
30	3.3 ± 0.2	30	3.2 ± 0.2
40	3.8 ± 0.2	40	3.8 ± 0.2
50	3.7 ± 0.2	50	4.1 ± 0.2

Table 16: Signal efficiencies in the four-prong $\tau^+\tau^-(h\to\tau^+\tau^-)$ and $\tau^+\tau^-(A\to\tau^+\tau^-)$ channels (LEP1).

mass (GeV/c^2)	efficiency (%)	mass (GeV/c^2)	efficiency (%)
m_h= 4	3.0 ± 0.2	m_A= 4	3.2 ± 0.2
7	5.3 ± 0.2	7	5.6 ± 0.2
9	5.8 ± 0.2	9	5.9 ± 0.2
10	6.0 ± 0.2	10	5.7 ± 0.2
12	6.3 ± 0.2	12	6.2 ± 0.2
15	5.9 ± 0.2	15	6.2 ± 0.2
20	6.1 ± 0.2	20	5.7 ± 0.2
30	6.2 ± 0.2	30	5.8 ± 0.2
40	6.5 ± 0.2	40	6.3 ± 0.2
50	6.2 ± 0.2	50	5.9 ± 0.2

Table 17: Signal efficiencies in the six-prong $\tau^+\tau^-(h\to\tau^+\tau^-)$ and $\tau^+\tau^-(A\to\tau^+\tau^-)$ channels (LEP1).

mass (GeV/c^2)	efficiency (%)	mass (GeV/c^2)	efficiency (%)
m_h= 4	2.4 ± 0.2	m_A= 4	2.5 ± 0.2
7	3.9 ± 0.2	7	4.3 ± 0.2
9	4.5 ± 0.2	9	4.6 ± 0.2
10	4.3 ± 0.2	10	4.6 ± 0.2
12	4.7 ± 0.2	12	4.6 ± 0.2
15	4.7 ± 0.2	15	4.8 ± 0.2
20	5.6 ± 0.2	20	4.8 ± 0.2
30	5.5 ± 0.2	30	5.4 ± 0.2
40	5.5 ± 0.2	40	5.3 ± 0.2
50	5.6 ± 0.2	50	5.2 ± 0.2

Table 18: Signal efficiencies in the $hA\to(AA)A\to6b$ channel (LEP2).

mass (GeV/c^2)	efficiency (%)				
m_A,m_h	$\sqrt{s}$ = 189 GeV	192 GeV	196 GeV	200 GeV	206 GeV
12,70	27.1 ± 1.6	26.9 ± 1.6	27.4 ± 1.7	27.3 ± 1.7	26.6 ± 1.6
12,90	44.2 ± 2.1	44.0 ± 2.1	44.1 ± 2.1	42.3 ± 2.1	41.8 ± 2.0
12,110	47.9 ± 2.2	48.1 ± 2.2	48.8 ± 2.2	49.6 ± 2.2	49.0 ± 2.2
12,130	42.8 ± 2.1	43.4 ± 2.1	44.4 ± 2.1	44.1 ± 2.1	44.0 ± 2.1
12,150	36.3 ± 1.9	38.1 ± 2.0	39.7 ± 2.0	41.0 ± 2.0	42.4 ± 2.1
12,170	4.2 ± 0.7	4.6 ± 0.7	5.9 ± 0.8	11.3 ± 1.1	22.7 ± 1.5
30,70	49.1 ± 2.2	49.6 ± 2.3	48.5 ± 2.2	49.0 ± 2.2	48.8 ± 2.2
30,90	52.5 ± 2.3	53.2 ± 2.3	53.7 ± 2.3	53.7 ± 2.3	53.7 ± 2.3
30,110	54.3 ± 2.3	54.2 ± 2.3	54.4 ± 2.3	54.5 ± 2.3	54.5 ± 2.3
30,130	53.2 ± 2.3	53.9 ± 2.3	53.9 ± 2.3	53.7 ± 2.3	53.6 ± 2.3
30,150	50.1 ± 2.3	49.8 ± 2.3	50.4 ± 2.3	51.0 ± 2.3	51.0 ± 2.3
50,110	56.3 ± 2.4	56.9 ± 2.4	57.9 ± 2.4	57.9 ± 2.4	57.9 ± 2.4
50,130	57.0 ± 2.4	57.9 ± 2.4	58.4 ± 2.4	58.5 ± 2.4	58.6 ± 2.4

Table 19: Signal efficiencies in the hZ→(AA)Z→4b+jets channel (LEP2).

mass (GeV/c^2)	efficiency (%)				
m_A,m_h	$\sqrt{s}$ = 189 GeV	192 GeV	196 GeV	200 GeV	206 GeV
12,30	6.9 ± 0.8	7.7 ± 0.9	8.3 ± 0.9	7.6 ± 0.9	8.3 ± 0.9
12,50	13.8 ± 1.2	13.8 ± 1.2	14.7 ± 1.2	14.8 ± 1.2	14.7 ± 1.2
12,70	20.7 ± 1.4	20.3 ± 1.4	19.9 ± 1.4	19.8 ± 1.4	20.2 ± 1.4
12,90	20.9 ± 1.4	21.8 ± 1.5	20.9 ± 1.4	21.0 ± 1.4	21.1 ± 1.5
12,105				23.0 ± 1.5	23.7 ± 1.5
20,50	13.0 ± 1.1	12.3 ± 1.1	12.2 ± 1.1	12.3 ± 1.1	12.3 ± 1.1
20,70	14.4 ± 1.2	14.4 ± 1.2	13.8 ± 1.2	13.8 ± 1.2	13.7 ± 1.2
20,90	19.0 ± 1.4	18.9 ± 1.4	18.4 ± 1.4	18.5 ± 1.4	18.4 ± 1.4
20,105				19.4 ± 1.4	21.1 ± 1.5
30,70	16.8 ± 1.3	17.0 ± 1.3	15.5 ± 1.3	15.6 ± 1.3	15.5 ± 1.3
30,90	21.9 ± 1.5	22.3 ± 1.5	22.2 ± 1.5	22.3 ± 1.5	22.3 ± 1.5
30,105				24.8 ± 1.6	24.8 ± 1.6
40,90	22.1 ± 1.6	22.4 ± 1.6	22.2 ± 1.6	22.3 ± 1.6	22.3 ± 1.6
40,105				26.1 ± 1.7	25.4 ± 1.7

Table 20: Signal efficiencies in the hA→h(hZ)→4b+jets channel (LEP2).

mass (GeV/c^2)	efficiency (%)				
m_A,m_h	$\sqrt{s}$ = 189 GeV	192 GeV	196 GeV	200 GeV	206 GeV
12,110	10.6 ± 1.0	10.6 ± 1.0	10.5 ± 1.0	10.6 ± 1.0	10.5 ± 1.0
12,130	14.6 ± 1.2	14.5 ± 1.2	14.8 ± 1.2	14.6 ± 1.2	15.4 ± 1.3
12,150	14.3 ± 1.2	14.1 ± 1.2	14.3 ± 1.2	14.9 ± 1.2	15.4 ± 1.3
12,170	10.8 ± 1.1	12.6 ± 1.2	13.5 ± 1.3	13.9 ± 1.3	14.2 ± 1.3
30,130	15.1 ± 1.3	15.1 ± 1.3	15.4 ± 1.3	15.7 ± 1.3	15.6 ± 1.3
30,150	15.8 ± 1.3	15.6 ± 1.3	16.0 ± 1.3	16.2 ± 1.3	16.2 ± 1.3

Table 21: Signal efficiencies in the hA→4b channel (LEP2). The efficiencies are symmetric in m_h and m_A.

mass (GeV/c^2)	efficiency (%)				
m_A,m_h	$\sqrt{s}$ = 189 GeV	192 GeV	196 GeV	200 GeV	206 GeV
12,50	2.5 ± 0.5	2.0 ± 0.4	1.6 ± 0.4	1.3 ± 0.4	1.3 ± 0.4
12,70	15.7 ± 1.3	15.3 ± 1.2	15.4 ± 1.2	15.4 ± 1.2	14.5 ± 1.2
12,90	25.4 ± 1.6	25.0 ± 1.6	24.8 ± 1.6	24.5 ± 1.6	23.6 ± 1.6
12,110	30.7 ± 1.8	31.8 ± 1.8	31.7 ± 1.8	31.4 ± 1.8	30.9 ± 1.8
12,130	30.5 ± 1.7	31.1 ± 1.8	30.6 ± 1.7	31.8 ± 1.8	31.3 ± 1.8
12,150	23.1 ± 1.5	23.8 ± 1.5	24.2 ± 1.6	25.2 ± 1.6	26.3 ± 1.6
12,170	8.6 ± 0.9	10.0 ± 1.0	11.7 ± 1.1	14.5 ± 1.2	17.1 ± 1.3
30,30	3.0 ± 0.5	3.0 ± 0.5	2.9 ± 0.5	2.8 ± 0.5	2.9 ± 0.5
30,50	16.0 ± 1.3	15.8 ± 1.3	15.2 ± 1.2	14.5 ± 1.2	14.1 ± 1.2
30,70	30.3 ± 1.7	30.4 ± 1.7	30.8 ± 1.8	30.3 ± 1.7	29.5 ± 1.7
30,90	35.1 ± 1.9	35.7 ± 1.9	35.0 ± 1.9	35.2 ± 1.9	35.3 ± 1.9
30,110	35.2 ± 1.9	35.6 ± 1.9	35.4 ± 1.9	34.6 ± 1.9	34.9 ± 1.9
30,130	31.9 ± 1.8	32.9 ± 1.8	33.7 ± 1.8	33.6 ± 1.8	34.3 ± 1.9
30,150	24.0 ± 1.5	26.4 ± 1.6	27.4 ± 1.7	27.0 ± 1.6	27.2 ± 1.6
50,50	33.7 ± 1.8	33.8 ± 1.8	33.7 ± 1.8	34.1 ± 1.8	33.5 ± 1.8
50,70	33.1 ± 1.8	33.7 ± 1.8	32.9 ± 1.8	32.8 ± 1.8	33.4 ± 1.8
50,90	37.4 ± 1.9	37.9 ± 1.9	38.7 ± 2.0	38.9 ± 2.0	39.2 ± 2.0
50,110	37.3 ± 1.9	37.3 ± 1.9	37.5 ± 1.9	37.3 ± 1.9	36.8 ± 1.9
50,130	31.8 ± 1.8	33.1 ± 1.8	34.4 ± 1.9	33.8 ± 1.8	34.7 ± 1.9
70,70	36.8 ± 1.9	37.3 ± 1.9	37.4 ± 1.9	37.5 ± 1.9	37.9 ± 1.9
70,90	41.2 ± 2.0	41.5 ± 2.0	41.7 ± 2.0	42.1 ± 2.1	42.5 ± 2.1
70,110	37.4 ± 1.9	37.9 ± 1.9	38.9 ± 2.0	38.3 ± 2.0	38.9 ± 2.0

Table 22: Signal efficiencies in the hA$\rightarrow 4\tau$ channel (examples given at $\sqrt{s}$=200 GeV). The efficiencies are symmetric in m_h and m_A.

mass (GeV/c^2)	efficiency (%)		
m_A,m_h	four-jet	three-jet	two-jet
4,4			37.0 ± 2.3
4,15			29.0 ± 2.2
4,35		10.6 ± 2.1	15.8 ± 2.2
4,50		11.9 ± 2.1	11.7 ± 2.1
4,70		28.4 ± 2.2	6.3 ± 2.1
4,90		43.4 ± 2.3	5.7 ± 2.1
4,125		44.7 ± 2.3	3.1 ± 2.0
4,170	4.0 ± 2.0	23.5 ± 2.2	4.7 ± 2.1
15,15	3.5 ± 2.0		19.1 ± 2.2
15,35	5.9 ± 2.1		14.3 ± 2.2
15,50	10.3 ± 2.1		12.9 ± 2.1
15,70	26.1 ± 2.2	2.3 ± 2.0	12.1 ± 2.1
15,90	32.7 ± 2.3	3.1 ± 2.0	11.3 ± 2.1
15,125	32.3 ± 2.3	2.2 ± 2.0	7.8 ± 2.1
15,170	18.1 ± 2.2	4.1 ± 2.0	8.4 ± 2.1
35,35	13.3 ± 2.1		12.7 ± 2.1
35,50	26.4 ± 2.2		11.3 ± 2.1
35,70	39.0 ± 2.3		10.4 ± 2.1
35,90	41.1 ± 2.3	2.3 ± 2.0	9.0 ± 2.1
35,125	38.6 ± 2.3	2.3 ± 2.0	7.6 ± 2.1
35,150	37.2 ± 2.3	3.0 ± 2.0	6.9 ± 2.1
50,50	38.7 ± 2.3		10.4 ± 2.1
50,70	43.5 ± 2.3	2.6 ± 2.0	9.2 ± 2.1
50,90	42.9 ± 2.3	2.6 ± 2.0	7.6 ± 2.1
50,135	43.2 ± 2.3	2.6 ± 2.0	6.1 ± 2.1
70,70	45.5 ± 2.3	2.5 ± 2.0	7.3 ± 2.1
70,90	49.5 ± 2.3	2.8 ± 2.0	5.4 ± 2.1
70,115	49.7 ± 2.3	3.5 ± 2.0	5.1 ± 2.1
90,90	49.4 ± 2.3	4.0 ± 2.1	5.2 ± 2.1

B Excluded couplings per process

This appendix contains tables of excluded couplings and suppression factors as functions of the involved Higgs boson masses, for all processes considered in this work. The mass granularity has been reduced in order to limit the size of the tables. `FORTRAN` routines containing the complete information can be obtained from the DELPHI collaboration on request.

Note that for the Yukawa process the results are given at the matrix element level rather than at the cross-section level (i.e. C instead of C^2); for all other cases the C^2 factors are listed. All masses are in GeV/c^2.

Table 23: **Yukawa channels:** upper bounds on the Yukawa C factors defined in Section 1.1, as function of m_h or m_A (GeV/c^2).

m_h,m_A	4	6	9	12	15	20	30	40	50
$C_{bb(h\rightarrow bb)}$				17.7	18.1	20.7	29.0	48.9	108.2
$C_{bb(A\rightarrow bb)}$				18.4	19.0	21.0	31.8	54.8	114.9
$C_{bb(h\rightarrow \tau\tau)}$	10.3	11.1	12.3	12.9	14.5	17.6	24.5	40.0	77.5
$C_{bb(A\rightarrow \tau\tau)}$	12.8	12.9	12.8	15.2	16.3	19.3	27.7	44.4	81.0
$C_{\tau\tau(h\rightarrow \tau\tau)}$	27.3	27.7	30.5	35.9	44.0	57.3	120.1		
$C_{\tau\tau(A\rightarrow \tau\tau)}$	29.4	28.5	31.7	37.8	44.8	62.1	128.1		

Table 24: **hA→4b:** upper bounds on $C^2_{hA\to 4b}$, combining the analyses presented here and the results of [5]. The results are given as a function of m_h and m_A (GeV/c^2), and are symmetric in m_h and m_A.

m_h,m_A	$C^2_{hA\to 4b}$	m_h,m_A	$C^2_{hA\to 4b}$	m_h,m_A	$C^2_{hA\to 4b}$	m_h,m_A	$C^2_{hA\to 4b}$
12,12	0.022	90,20	0.322	90,35	0.268	65,55	0.087
15,12	0.011	95,20	0.357	95,35	0.302	70,55	0.114
20,12	0.005	100,20	0.409	100,35	0.264	75,55	0.137
25,12	0.005	105,20	0.423	105,35	0.290	80,55	0.188
30,12	0.005	110,20	0.515	110,35	0.404	85,55	0.261
35,12	0.007	115,20	0.628	115,35	0.525	90,55	0.260
40,12	0.009	120,20	0.727	120,35	0.671	95,55	0.308
45,12	0.011	125,20	0.878	125,35	0.862	100,55	0.368
50,12	0.015	130,20	≥1	130,35	≥1	105,55	0.438
55,12	0.025	25,25	0.003	40,40	0.022	110,55	0.582
60,12	0.048	30,25	0.003	45,40	0.043	115,55	0.830
65,12	0.114	35,25	0.006	50,40	0.057	120,55	≥1
70,12	0.255	40,25	0.007	55,40	0.060	60,60	0.085
75,12	0.318	45,25	0.012	60,40	0.089	65,60	0.108
80,12	0.335	50,25	0.017	65,40	0.084	70,60	0.123
85,12	0.347	55,25	0.040	70,40	0.126	75,60	0.174
90,12	0.355	60,25	0.109	75,40	0.130	80,60	0.187
95,12	0.380	65,25	0.247	80,40	0.157	85,60	0.203
100,12	0.406	70,25	0.235	85,40	0.187	90,60	0.266
105,12	0.445	75,25	0.253	90,40	0.188	95,60	0.327
110,12	0.471	80,25	0.262	95,40	0.216	100,60	0.383
115,12	0.574	85,25	0.287	100,40	0.248	105,60	0.495
120,12	0.671	90,25	0.316	105,40	0.363	110,60	0.666
125,12	0.819	95,25	0.370	110,40	0.433	115,60	0.988
130,12	≥1	100,25	0.387	115,40	0.554	120,60	≥1
15,15	0.004	105,25	0.490	120,40	0.728	65,65	0.123
20,15	0.003	110,25	0.537	125,40	0.965	70,65	0.165
25,15	0.003	115,25	0.652	130,40	≥1	75,65	0.169
30,15	0.004	120,25	0.843	45,45	0.071	80,65	0.162
35,15	0.005	125,25	≥1	50,45	0.065	85,65	0.208
40,15	0.007	30,30	0.005	55,45	0.063	90,65	0.234
45,15	0.010	35,30	0.006	60,45	0.072	95,65	0.353
50,15	0.013	40,30	0.010	65,45	0.083	100,65	0.417
55,15	0.025	45,30	0.015	70,45	0.082	105,65	0.598
60,15	0.048	50,30	0.023	75,45	0.149	110,65	0.947
65,15	0.120	55,30	0.049	80,45	0.209	115,65	≥1
70,15	0.264	60,30	0.109	85,45	0.191	70,70	0.163
75,15	0.320	65,30	0.111	90,45	0.223	75,70	0.155
80,15	0.326	70,30	0.166	95,45	0.218	80,70	0.160
85,15	0.331	75,30	0.223	100,45	0.331	85,70	0.218
90,15	0.341	803,0	0.247	105,45	0.371	90,70	0.226
95,15	0.378	85,30	0.268	110,45	0.468	95,70	0.337
100,15	0.408	90,30	0.258	115,45	0.606	100,70	0.477
105,15	0.447	95,30	0.299	120,45	0.812	105,70	0.722
110,15	0.476	100,30	0.354	125,45	≥1	110,70	≥1
115,15	0.569	105,30	0.392	50,50	0.060	75,75	0.164
120,15	0.685	110,30	0.375	55,50	0.056	80,75	0.179
125,15	0.841	115,30	0.444	60,50	0.054	85,75	0.228
130,15	≥1	120,30	0.559	65,50	0.069	90,75	0.242
20,20	0.002	125,30	0.711	70,50	0.089	95,75	0.430
25,20	0.002	130,30	0.918	75,50	0.128	100,75	0.658
30,20	0.003	135,30	≥1	80,50	0.229	105,75	≥1
35,20	0.004	35,35	0.009	85,50	0.239	80,80	0.171
40,20	0.006	40,35	0.014	90,50	0.267	85,80	0.237
45,20	0.008	45,35	0.024	95,50	0.285	90,80	0.306
50,20	0.013	50,35	0.045	100,50	0.372	95,80	0.482
55,20	0.025	55,35	0.088	105,50	0.444	100,80	0.913
60,20	0.059	60,35	0.092	110,50	0.496	105,80	≥1
65,20	0.162	65,35	0.139	115,50	0.668	85,85	0.273
70,20	0.273	70,35	0.119	120,50	0.927	90,85	0.415
75,20	0.288	75,35	0.209	125,50	≥1	95,85	0.818
80,20	0.301	80,35	0.253	55,55	0.051	100,85	≥1
85,20	0.301	85,35	0.267	60,55	0.058	90,90	0.849

Table 25: **hA→4τ:** upper bounds on $C^2_{hA\to 4\tau}$, combining the two-jet, three-jet and four-jet streams. The results are given as a function of m_h and m_A (GeV/c^2), and are symmetric in m_h and m_A.

m_h,m_A	$C^2_{hA\to 4\tau}$	m_h,m_A	$C^2_{hA\to 4\tau}$	m_h,m_A	$C^2_{hA\to 4\tau}$	m_h,m_A	$C^2_{hA\to 4\tau}$
5,5	0.005	70,15	0.036	55,30	0.040	125,45	0.341
10,5	0.005	80,15	0.046	60,30	0.043	130,45	0.403
15,5	0.010	90,15	0.052	65,30	0.044	135,45	0.624
20,5	0.012	100,15	0.067	70,30	0.043	140,45	$\geq$1
25,5	0.010	110,15	0.091	80,30	0.048	50,50	0.038
30,5	0.012	115,15	0.111	90,30	0.056	55,50	0.041
35,5	0.017	120,15	0.134	100,30	0.075	60,50	0.043
40,5	0.021	125,15	0.163	110,30	0.106	65,50	0.045
45,5	0.027	130,15	0.206	115,30	0.126	70,50	0.048
50,5	0.032	135,15	0.270	120,30	0.156	80,50	0.061
55,5	0.033	140,15	0.366	125,30	0.196	90,50	0.081
60,5	0.031	145,15	0.502	130,30	0.246	100,50	0.115
65,5	0.034	150,15	0.711	135,30	0.335	110,50	0.175
70,5	0.037	155,15	$\geq$1	140,30	0.463	115,50	0.212
80,5	0.050	20,20	0.007	145,30	0.665	120,50	0.292
90,5	0.059	25,20	0.009	150,30	$\geq$1	125,50	0.402
100,5	0.074	30,20	0.010	35,35	0.021	130,50	0.637
110,5	0.104	35,20	0.017	40,35	0.023	135,50	0.884
115,5	0.125	40,20	0.016	45,35	0.031	140,50	$\geq$1
120,5	0.140	45,20	0.025	50,35	0.039	55,55	0.041
125,5	0.152	50,20	0.025	55,35	0.046	60,55	0.044
130,5	0.170	55,20	0.030	60,35	0.045	65,55	0.046
135,5	0.215	60,20	0.035	65,35	0.044	70,55	0.049
140,5	0.270	65,20	0.041	70,35	0.043	80,55	0.067
145,5	0.356	70,20	0.041	80,35	0.052	90,55	0.088
150,5	0.498	80,20	0.047	90,35	0.059	100,55	0.128
155,5	0.847	90,20	0.053	100,35	0.080	110,55	0.212
160,5	$\geq$1	100,20	0.069	110,35	0.115	115,55	0.288
10,10	0.006	110,20	0.094	115,35	0.139	120,55	0.395
15,10	0.011	115,20	0.122	120,35	0.172	125,55	0.536
20,10	0.007	120,20	0.142	125,35	0.220	130,55	0.929
25,10	0.010	125,20	0.169	130,35	0.273	135,55	$\geq$1
30,10	0.015	130,20	0.209	135,35	0.383	60,60	0.043
35,10	0.016	135,20	0.308	140,35	0.534	65,60	0.048
40,10	0.018	140,20	0.387	145,35	0.851	70,60	0.054
45,10	0.025	145,20	0.530	150,35	$\geq$1	80,60	0.072
50,10	0.040	150,20	0.751	40,40	0.025	90,60	0.097
55,10	0.043	155,20	$\geq$1	45,40	0.033	100,60	0.151
60,10	0.044	25,25	0.008	50,40	0.040	110,60	0.263
65,10	0.043	30,25	0.013	55,40	0.046	115,60	0.395
70,10	0.041	35,25	0.017	60,40	0.044	120,60	0.572
80,10	0.052	40,25	0.018	65,40	0.043	125,60	0.773
90,10	0.064	45,25	0.024	70,40	0.043	130,60	$\geq$1
100,10	0.068	50,25	0.029	80,40	0.055	65,65	0.053
110,10	0.089	55,25	0.035	90,40	0.067	70,65	0.060
115,10	0.110	60,25	0.041	100,40	0.093	80,65	0.079
120,10	0.123	65,25	0.044	110,40	0.129	90,65	0.111
125,10	0.135	70,25	0.043	115,40	0.150	100,65	0.175
130,10	0.177	80,25	0.052	120,40	0.184	110,65	0.333
135,10	0.214	90,25	0.054	125,40	0.250	115,65	0.555
140,10	0.265	100,25	0.062	130,40	0.330	120,65	$\geq$1
145,10	0.372	110,25	0.099	135,40	0.461	70,70	0.066
150,10	0.513	115,25	0.119	140,40	0.688	80,70	0.087
155,10	0.779	120,25	0.144	155,40	$\geq$1	90,70	0.128
160,10	$\geq$1	125,25	0.180	45,45	0.038	100,70	0.212
15,15	0.006	130,25	0.228	50,45	0.039	110,70	0.435
20,15	0.007	135,25	0.298	55,45	0.043	115,70	0.728
25,15	0.009	140,25	0.420	60,45	0.043	120,70	$\geq$1
30,15	0.011	145,25	0.582	65,45	0.043	80,80	0.117
35,15	0.014	150,25	0.843	70,45	0.045	90,80	0.207
40,15	0.020	155,25	$\geq$1	80,45	0.056	100,80	0.433
45,15	0.022	30,30	0.013	90,45	0.074	115,80	$\geq$1
50,15	0.024	35,30	0.019	100,45	0.102	90,90	0.417
55,15	0.029	40,30	0.020	110,45	0.150	110,90	$\geq$1
60,15	0.033	45,30	0.025	115,45	0.186	100,100	$\geq$1
65,15	0.036	50,30	0.028	120,45	0.237		

Table 26: **hZ→$\tau^+\tau^-$Z:** upper bounds on $C^2_{Z(h\to\tau\tau)}$, as function of m_h (GeV/c^2), reinterpreting the search for the Standard Model Higgs boson [5].

m_h	$C^2_{Z(h\to\tau\tau)}$	m_h	$C^2_{Z(h\to\tau\tau)}$	m_h	$C^2_{Z(h\to\tau\tau)}$	m_h	$C^2_{Z(h\to\tau\tau)}$	m_h	$C^2_{Z(h\to\tau\tau)}$
12	0.285	35	1.132	60	0.169	85	0.088	110	0.590
15	0.316	40	1.022	65	0.093	90	0.102	115	≥1
20	0.398	45	0.457	70	0.082	95	0.164		
25	0.530	50	0.260	75	0.095	100	0.219		
30	0.751	55	0.199	80	0.067	105	0.297		

Table 27: **hZ→b$\bar{\text{b}}$Z:** upper bounds on $C^2_{Z(h\to bb)}$, as function of m_h (GeV/c^2), reinterpreting the search for the Standard Model Higgs boson [5].

m_h	$C^2_{Z(h\to bb)}$	m_h	$C^2_{Z(h\to bb)}$	m_h	$C^2_{Z(h\to bb)}$	m_h	$C^2_{Z(h\to bb)}$	m_h	$C^2_{Z(h\to bb)}$
12	0.042	35	0.047	60	0.049	85	0.103	110	0.314
15	0.046	40	0.060	65	0.035	90	0.176	115	≥1
20	0.047	45	0.064	70	0.034	95	0.262		
25	0.054	50	0.046	75	0.040	100	0.273		
30	0.063	55	0.047	80	0.055	105	0.215		

Table 28: **hA→6b:** upper bounds on $C^2_{hA\to 6b}$, as a function of m_h and m_A (GeV/c^2).

m_h,m_A	$C^2_{hA\to 6b}$	m_h,m_A	$C^2_{hA\to 6b}$	m_h,m_A	$C^2_{hA\to 6b}$	m_h,m_A	$C^2_{hA\to 6b}$
25,12	≥1	95,15	0.242	80,25	0.176	110,35	0.396
30,12	≥1	100,15	0.265	85,25	0.193	115,35	0.478
35,12	≥1	105,15	0.296	90,25	0.211	120,35	0.581
40,12	0.879	110,15	0.327	95,25	0.235	125,35	0.736
45,12	0.701	115,15	0.391	100,25	0.261	130,35	0.949
50,12	0.625	120,15	0.471	105,25	0.299	135,35	≥1
55,12	0.256	125,15	0.571	110,25	0.339	80,40	0.195
60,12	0.189	130,15	0.733	115,25	0.410	85,40	0.216
65,12	0.183	135,15	0.898	120,25	0.503	90,40	0.299
70,12	0.181	140,15	≥1	125,25	0.614	95,40	0.273
75,12	0.209	40,20	0.547	130,25	0.764	100,40	0.320
80,12	0.213	45,20	0.155	135,25	0.997	105,40	0.365
85,12	0.217	50,20	0.098	140,25	≥1	110,40	0.440
90,12	0.218	55,20	0.125	60,30	0.141	115,40	0.535
95,12	0.240	60,20	0.146	65,30	0.150	120,40	0.699
100,12	0.261	65,20	0.168	70,30	0.149	125,40	0.866
105,12	0.292	70,20	0.173	75,30	0.165	130,40	≥1
110,12	0.322	75,20	0.193	80,30	0.175	90,45	0.264
115,12	0.390	80,20	0.206	85,30	0.194	95,45	0.300
120,12	0.466	85,20	0.191	90,30	0.210	100,45	0.349
125,12	0.586	90,20	0.210	95,30	0.234	105,45	0.410
130,12	0.725	95,20	0.234	100,30	0.270	110,45	0.493
135,12	0.922	100,20	0.265	105,30	0.313	115,45	0.616
140,12	≥1	105,20	0.294	110,30	0.361	120,45	0.786
30,15	≥1	110,20	0.333	115,30	0.428	125,45	≥1
35,15	≥1	115,20	0.390	120,30	0.524	100,50	0.391
40,15	0.713	120,20	0.474	125,30	0.654	105,50	0.469
45,15	0.177	125,20	0.593	130,30	0.826	110,50	0.571
50,15	0.195	130,20	0.723	135,30	≥1	115,50	0.733
55,15	0.202	135,20	0.938	70,35	0.159	120,50	0.956
60,15	0.169	140,20	≥1	75,35	0.168	125,50	≥1
65,15	0.179	50,25	0.111	80,35	0.189	110,55	0.688
70,15	0.178	55,25	0.129	85,35	0.206	115,55	0.907
75,15	0.214	60,25	0.134	90,35	0.226	120,55	≥1
80,15	0.211	65,25	0.169	95,35	0.253	120,60	≥1
85,15	0.213	70,25	0.161	100,35	0.289		
90,15	0.215	75,25	0.178	105,35	0.335		

Table 29: **hZ → 4b+jets:** upper bounds on $C^2_{Z(AA\to 4b)}$, as a function of m_h and m_A (GeV/c^2).

m_h,m_A	$C^2_{Z(AA\to 4b)}$	m_h,m_A	$C^2_{Z(AA\to 4b)}$	m_h,m_A	$C^2_{Z(AA\to 4b)}$	m_h,m_A	$C^2_{Z(AA\to 4b)}$
25,12	$\geq$1	55,15	0.244	95,20	0.696	95,30	0.579
30,12	0.324	60,15	0.252	100,20	0.947	100,30	0.776
35,12	0.281	65,15	0.240	110,20	$\geq$1	110,30	$\geq$1
40,12	0.250	70,15	0.262	50,25	0.253	70,35	0.273
45,12	0.230	75,15	0.273	55,25	0.262	75,35	0.287
50,12	0.218	80,15	0.302	60,25	0.273	80,35	0.296
55,12	0.216	85,15	0.372	65,25	0.289	85,35	0.338
60,12	0.219	90,15	0.434	70,25	0.313	90,35	0.392
65,12	0.221	95,15	0.641	75,25	0.314	95,35	0.567
70,12	0.231	100,15	0.869	80,25	0.319	100,35	0.771
75,12	0.258	110,15	$\geq$1	85,25	0.367	110,35	$\geq$1
80,12	0.289	40,20	0.267	90,25	0.426	80,40	0.292
85,12	0.338	45,20	0.266	95,25	0.632	85,40	0.330
90,12	0.417	50,20	0.266	100,25	0.856	90,40	0.391
95,12	0.612	55,20	0.276	110,25	$\geq$1	95,40	0.570
100,12	0.829	60,20	0.290	60,30	0.260	100,40	0.759
110,12	$\geq$1	65,20	0.311	65,30	0.276	110,40	$\geq$1
30,15	0.303	70,20	0.333	70,30	0.292	90,45	0.503
35,15	0.295	75,20	0.344	75,30	0.296	95,45	0.586
40,15	0.276	80,20	0.363	80,30	0.314	100,45	$\geq$1
45,15	0.250	85,20	0.401	85,30	0.340	100,50	$\geq$1
50,15	0.233	90,20	0.467	90,30	0.393	110,55	$\geq$1